

Thermodynamic principles of emerging cryopreservation technologies

Matthew J. Powell-Palm^{1,2,3,4} and Anthony N. Consiglio^{4,5}

¹ J. Mike Walker '66 Department of Mechanical Engineering, Texas A&M University, College Station, TX, USA

² Department of Materials Science & Engineering, Texas A&M University, College Station, TX, USA

³ Department of Biomedical Engineering, Texas A&M University, College Station, TX, USA

⁴ BioChoric Inc., Bozeman, MT, USA

⁵ Department of Mechanical Engineering, University of California, Berkeley, Berkeley, CA, USA,

powellpalm@tamu.edu,

aconsiglio4@berkeley.edu

Abstract. Modern cryopreservation exists at the convergence of diverse disciplines—materials science, physical chemistry, mechanical engineering, biological engineering, etc.—and emerging technologies often draw from many of these disciplines simultaneously. Thermodynamics, as one of the foundational theories underlying both physical and biological science, provides a framework through which to understand these interdisciplinary technologies, yet the full kit of requisite thermodynamic tools is not housed within any one discipline. This Chapter aims to articulate a foundational thermodynamic approach to the description, interrogation, and design of modern cryopreservation technologies, and to review the state of the art in emerging cryopreservation technologies through the lens of this approach. We focus in particular on the management of phase change across equilibrium-driven techniques (e.g. liquidus tracking, partial freezing, isochoric freezing), kinetics-driven techniques (e.g. supercooling, ice seeding), and transport-driven techniques (e.g. directional freezing, droplet approaches), and we hope to equip the reader with a self-consistent theoretical toolkit that enables meaningful comparison of these techniques from a thermodynamic perspective.

Keywords: Cryopreservation technologies, Solution thermodynamics, Ice nucleation, Supercooling, Isochoric freezing, Partial Freezing, Liquidus tracking, Directional freezing

Preprint acknowledgment

This is a preprint of the following chapter: Matthew J. Powell-Palm and Anthony N. Consiglio, Thermodynamic principles of emerging cryopreservation technologies, published in *Cryopreservation and Freeze-Drying Protocols*, edited by Willem F. Wolkers and Harriëtte Oldenhof, 2026, Springer. It is the version of the author's manuscript prior to acceptance for publication and has not undergone editorial and/or peer review on behalf of the Publisher (where applicable).

1 Introduction

Effective cryopreservation of biological matter—be that matter a cell, a tissue, an organ, or an organism—hinges upon the uniquely complicated interplay between the thermodynamics of aqueous solutions, the nucleation and growth kinetics of ice and other solid phases, and the transport of heat and mass through spatially and chemically heterogeneous media. As such, mathematical description, interrogation, and design of cryopreservation processes require a uniquely varied blend of physical theories, drawn from disciplines ranging from physical chemistry and atmospheric science to mechanical engineering and materials science. Classical geometric (or Gibbsian) thermodynamics can provide a unifying framework to connect these disparate bases of knowledge, but reconciliation of different schools of thermodynamic practice in the context of cryopreservation is required.

To that end, in this Chapter, we will present a thermodynamic description of the physical aspects of cryopreservation, enabling self-consistent interrogation of the physical bases of various emergent cryopreservation technologies. In the first Section, we will establish this description in additive sub-sections focusing on solution thermodynamics, ice nucleation & growth kinetics, and heat and mass transport. In each sub-section, we will aim to equip the user firstly with high-level physical insight applicable to emergent cryopreservation technologies, and secondly with basic predictive power over the same. In the second Section, we will review various such technologies within the context of our unified physical framework, aiming to facilitate interrogation of how the underlying thermodynamic premise of each technology may resemble or differ from the others.

For consistency with our theoretical approach, we will group these emergent technologies by the theoretical aspect—equilibrium thermodynamics, kinetics, or transport—that most principally drives them. For example, liquidus tracking, partial freezing [1], and isochoric freezing [2] all rely upon attainment of a desired state of thermodynamic equilibrium, wherein ice may be either entirely absent (liquidus tracking) or allowed to an extent prescribed by the liquidus equilibria of the solution (partial freezing and isochoric freezing). Supercooling [3] and ice seeding, by comparison, rely upon attainment of a desired nucleation rate (supercooling) or ice growth rate (seeding), which, while of course influenced by the underlying phase equilibria, are ultimately kinetic factors. Likewise, various other techniques rely upon attainment of a desired temperature profile *en route* to the final state of preservation, be it a profile in time (as in droplet and mesh technologies that seek to amplify cooling rates) or in space (as in directional freezing). These techniques are no less subject to the relevant phase equilibria and nucleation kinetics, but they additionally leverage transport phenomena to optimize (and in many cases circumvent) aspects of those factors.

Throughout this Chapter, we will treat these many technologies from a principally physical perspective, and we will adopt to a significant degree the terminology and philosophy of Gibbsian geometric thermodynamics. For a robust introduction to this school of thought, we recommend the seminal textbook of Herbert Callen [4].

2 Thermodynamic and physical principles of ice management in cryopreservation

Cryopreservation, at its most fundamental, seeks to manipulate the state and action of water in and around a biological specimen such that mechanical, chemical, and biological damage are avoided at those sub-normothermic temperatures at which the processes of life are slowed or arrested. While the toxicological challenge of cryopreservation is concerned principally with the biochemical action of this water, the physical challenge of cryopreservation most often involves the *phase* of this water, and its tendency to change in undesirable ways upon cooling to the sub-0 °C temperatures at which the slowing of life processes becomes sufficient to enable days-, weeks-, or years-long preservation. As such, our physical description of cryopreservation is first and foremost a description of the unique behaviors of liquid water and solid ice, in the presence of various chemicals, under various temperatures and pressures, in contact with various surfaces, and subject to various gradients in time, space, energy, and matter. We will group this description into three sub-sections, treating relevant aspects of the equilibrium thermodynamics, ice nucleation and growth kinetics, and heat and mass transport at play.

2.1 Equilibrium thermodynamics

We begin our description of the thermodynamics of cryopreservation with the most fundamental quantity dictating the response of water and ice to these varying conditions: the chemical potential, μ . The chemical

potential, or the rate at which the free energy of a substance changes with the addition of more of that substance to a system, is the thermodynamic parameter most responsible for directing the action of water. It dictates both whether water can (and in part whether it *will*) change phase from a liquid to a solid; it dictates the extent to which (and in part *the speed* with which) crystalline ice will grow upon nucleation; and it dictates whether (and in part *how quickly*) water will migrate by diffusion or osmosis. As such, description of the chemical potential is the first step in formulating our broader description of physical cryopreservation.

2.1.1 The chemical potential

The chemical potential of a component i is defined as:

$$\mu_i = \left(\frac{\partial G}{\partial N_i} \right)_{T, p, N_j \neq i} \quad (1)$$

Wherein G gives the Gibbs free energy of the system, N_i is the number of mols of component i , and subscripts outside the differentials indicate variables held constant. μ_i is most typically given in units of J/mol, and it is an intensive thermodynamic variable, which means that it is scale-invariant, and it provides a driving force for equilibration among chemical species. Analogous to how differences in temperature compel the flow of heat and differences in pressure compel the flow of volume, differences in chemical potential compel the flow of molecules, be they into new phases (as in the formation of ice) or into new locations (as in osmosis or diffusion).

For pure water (or any pure substance), the chemical potential is simply equal to the Gibbs free energy per mol. For liquid water, common hexagonal ice (ice Ih), and several high-pressure ice polymorphs, this quantity has been rigorously measured across a wide range of temperatures and pressures and parameterized into powerful and accessible equations of state. Throughout this work, we will use the open-source SeaFreeze [5] package maintained by Journaux and colleagues.

Thermodynamic equilibrium in a cryobiological system consisting of different phases (or alternatively compartments) 1 and 2 requires the condition of equality of the intensive thermodynamic variables ($\mu_1 = \mu_2$, $p_1 = p_2$, $T_1 = T_2$). Practically speaking, these conditions state that, at a given pressure, at the phase transition temperature, wherein the two phases at hand are definitionally in equilibrium, their chemical potentials must be equal. We refer to the set of interrelated intensive variables that define equilibrium between two or more phases as phase equilibria, or equilibrium coordinates.

In cryobiological problems, calculation of the chemical potential is used for three principal purposes: 1) to solve for the temperature (and/or pressure) at which water and ice are in equilibrium in a given solution, i.e. to calculate the composition-dependent melting point of ice, 2) to calculate the driving force for ice nucleation (discussed in later sections), and 3) to calculate the driving force for mass transfer during CPA loading (discussed in later sections).

2.1.2 Solution theories

As stated, in the modern era, the chemical potentials of pure water and pure ice are well known - the challenge of cryopreservation thus falls to describing how the chemical potential of water *changes* in the presence of the myriad biologically-necessary or cryoprotective molecules, i.e. in solution. Armed with this knowledge, because the chemical potential of ice does not change with solution composition (given that ice rejects solutes and forms an approximately pure crystal), liquid-ice phase equilibria may be readily determined by equating the calculated chemical potential of water in solution with the known chemical potential of ice and solving for the temperature-pressure-concentration conditions that yield that equality.

To calculate this chemical potential, we utilize geometric or Gibbsian solution thermodynamics. Originally derived in the late 19th and early 20th centuries by Gibbs, Raoult, Lewis, Hildebrand, and others, and today practiced in many distinct varieties, the Gibbsian school of solution thermodynamics generally treats the free energy of a solution G as a mol-weighted average of the free energy of its constituent components plus a term capturing the effects of mixing these components together, such that

$$G = \sum_i N_i \mu_i^0 + \Delta G_{\text{mix}} \quad (2)$$

Generally, ΔG_{mix} aims to capture the effects of entropy that accompany mixing arbitrary components together (the entropy of mixing ΔS_{mix}) and the molecular interactions that may occur between the

components (the enthalpy of mixing ΔH_{mix}), such that $\Delta G_{\text{mix}} = \Delta H_{\text{mix}} - T \Delta S_{\text{mix}}$. While this framework is more or less universal within Gibbsian thermodynamics, specific solution theories proceed to quantify ΔG_{mix} in a variety of different ways, requiring different degrees of experimental input and yielding different predictive and descriptive powers. We will discuss here three key theories, chosen for their particular applicability to problems of cryobiology and their extensibility to multi-solute solutions.

The simplest theory of solutions is the ideal model, which assumes that the different components in solution do not interact whatsoever ($\Delta H_{\text{mix}} = 0$), and that, for entropic purposes, the molecules may be treated as physically identical. In this case, the entropy of mixing (in units of Joules per Kelvin) is given by

$$\Delta S_{\text{mix}}^{\text{ideal}} = -R \sum_i N_i \ln x_i \quad (3)$$

The Gibbs free energy of the solution is then

$$G = \sum_i N_i \mu_i^0 + RT \sum_i N_i \ln x_i \quad (4)$$

and the chemical potential of component i in an ideal solution is

$$\mu_i = \mu_i^0 + RT \ln x_i \quad (5)$$

Critically, this result implies that, within the ideal conception, the chemical potential of a given component is compositionally dependent only on *its own* concentration, and agnostic to the specific solutes accompanying it in solution. As cryobiologists surely appreciate, this agnosticism does not bear out experimentally, considering that different cryoprotectants in reality depress the melting point of water to very differing degrees at the same molar concentration.

The ideal model is thus limited in empirical accuracy but has nonetheless proven an invaluable exploratory tool for the interrogation of generalized effects of composition on various physical processes. This utility is driven both by its simplicity and its reliance only on properties of the *pure* components, as opposed to properties of the solution itself, which enables *predictive* exploration of new solutions without synthesizing the desired solution and measuring some subset of its properties. Furthermore, the ideal model is readily extensible to arbitrarily complex n -component solutions.

Recently, Alliston et al. [6] introduced a modification to the ideal model (the size-dependent ideal solution or SIS model) to incorporate solute-specific size information whilst retaining the predictive, parameter-free nature of the ideal solution theory and its easy extensibility to multi-component mixtures. Based on statistical mechanics arguments by Flory [7] and Hildebrand [8] and kinetic observations by Powell-Palm et al. [9], Alliston et al. replace the ideal entropy of mixing with a size-dependent entropy of mixing capturing the entropic impact of the considerable size difference between water and typical organic cryoprotectants, which often possesses $\sim 4\text{--}10$ times the molar volume of water. For a solution of components i with molar volumes v_i , and volume fraction ϕ_i , the SIS mixing entropy is

$$\Delta S_{\text{mix}}^{\text{SIS}} = -R \sum_i N_i \ln \left(\frac{v_i N_i}{\sum_j v_j N_j} \right) = -R \sum_i N_i \ln \phi_i \quad (6)$$

Substituting this entropy into the expression for the Gibbs free energy and differentiating, one obtains a size-dependent chemical potential. For a general multicomponent mixture, this can be written compactly as:

$$\frac{\mu_i - \mu_i^0}{RT} = \ln \phi_i + \sum_{j \neq i} (1 - r_{ij}) \phi_j \quad (7)$$

where $r_{ij} = v_i/v_j$ is the ratio of molar volumes. Using only bulk-material molar volumes at room temperature, the incorporation of this simple size-dependence has been shown to increase the accuracy of the ideal model by $\sim 50\%$ or more for binary solutions of water and cryopreservation-relevant organic molecules, both in calculation of the melting point of ice in solution and in identification of solubility limits and eutectic temperatures/compositions.

While the above theories are purely *predictive*, requiring no experimental knowledge of the solution of interest, more accurate theories can be developed using experimental input measured from a few discrete concentrations. Many such descriptive theories start from the standard definitions:

$$\mu_i = \mu_i^0 + RT \ln a_i \quad (8)$$

$$\gamma_i = \frac{a_i}{x_i} \quad (9)$$

wherein a_i denotes the activity and γ_i the activity coefficient of component i in solution, and is a function of both composition, temperature, and pressure (though the dependence on temperature and pressure is often very weak). The activity coefficient of a component is an empirical measure of its deviation from ideality (as $\gamma^{\text{ideal}} = 1$), and activity-based descriptive theories typically seek to prescribe how γ_i varies with composition.

A convenient unifying language for many non-ideal models is the excess free energy approach, which considers the free energy as the sum of ideal and excess contributions: $G/N = g = g^{\text{ideal}} + g^{\text{excess}}$. The activity coefficient is thus given by

$$\ln \gamma_i = \frac{1}{RT} \left(\frac{\partial G^{\text{excess}}}{\partial N_i} \right)_{T,p,N_j \neq i} \quad (10)$$

The ideal Gibbs free energy is given in Equation 4 and the ideal entropy is given in Equation 3. The size-dependent ideal solution theory, which maintains zero excess enthalpy, has excess entropy ($Ts^E = h^E - g^E$) and water activity coefficient of

$$s^{\text{E,SIS}} = -R \sum_i x_i \ln \left(\frac{\phi_i}{x_i} \right) \quad (11)$$

$$\ln \gamma_w^{\text{SIS}} = \ln \left(\frac{\phi_w}{x_w} \right) + \sum_i \left(1 - \frac{v_w}{v_i} \right) \phi_i \quad (12)$$

The regular solution theory represents the simplest energetic extension of the ideal solution theory. In its conventional form, it assumes zero excess *entropy* (no size-dependence), but allows for nonzero *enthalpy* of mixing, typically represented in terms of binary interaction parameters, χ_{ij} , between each pair of species. The excess enthalpy and water activity coefficient for a regular solution can be written as

$$h^{\text{E,regular}} = \frac{1}{2} RT \sum_{i,j} \chi_{ij} x_i x_j \quad (13)$$

$$\ln \gamma_w^{\text{regular}} = \sum_i \chi_{wi} x_i^2 + \sum_{j>i} (\chi_{wi} + \chi_{wj} + \chi_{ij}) x_i x_j \quad (14)$$

For binary systems this reduces to the familiar symmetric form involving a single χ parameter. In practice, the χ_{ij} are fitted to empirical data such as freezing points or vapor pressures. In the context of cryobiology, regular solutions are rarely used in their full generality, but the underlying idea of augmenting the ideal or SIS baseline with simple energetic interaction terms underpins many common approaches.

In cryobiological systems, the chemical potential of water is of primary interest; the activities of the other solutes are needed in fewer instances. It is therefore common to express the state of water in solution by the parameters known as osmolality and osmotic pressure. Osmolality is directly related to the chemical potential of water and the water activity by

$$\pi = -\frac{\ln a_w}{M_w} = \frac{\mu_w^0 - \mu_w}{M_w RT} \quad (15)$$

where M_w is the molecular weight of water. Normal physiological osmolality lies approximately in the range 280-300 mOsm/kg. The corresponding osmotic pressure is related to π via

$$\Pi = \pi \rho_w RT \quad (16)$$

with ρ_w the density of water. Normal physiological osmotic pressure (at 37 °C) is approximately 7–8 atm.

A particularly useful implementation of regular solution theory pioneered by Elliott and colleagues for cryobiologically-relevant mixtures is the osmotic virial equation [10–12]. In this model, the osmolality is expanded as a polynomial in terms of solute molalities, m_i :

$$\pi = \sum_i k_i m_i + \sum_{i,j} \frac{B_i + B_j}{2} k_i m_i k_j m_j + \sum_{i,j,k} (C_i C_j C_k)^{1/3} k_i m_i k_j m_j k_k m_k \quad (17)$$

Here, k_i is the dissociation constant (capturing ionic dissociation of electrolytes), and B_i and C_i are the first and second virial coefficients encapsulating pairwise and triplet interactions between solutes. For each solute, the parameters k_i , B_i , and C_i are obtained by fitting single-solute osmotic or freezing-point data; multisolute behavior is then predicted via combining rules analogous to those used in regular solution theory. Requiring only binary parameters to describe multi-component solutions, the osmotic virial equation has become a workhorse solution theory for many cryobiological modeling efforts.

Beyond the models emphasized here, a wide variety of more elaborate solution theories have been developed which could be of use to cryobiological problems. These include classical local-composition models such as NRTL [13] (non-random two-liquid; and extensions such as eNRTL) and UNIQUAC¹³ (universal quasi-chemical); group contribution methods built upon these such as UNIFAC¹³ (UNIQUAC functional-group activity coefficients) and AIOMFAC [14] (aerosol inorganic-organic mixtures functional group activity coefficients); and quantum-chemical models such as COSMO-RS [15, 16] and COSMO-SAC [17] (conductor-like screening model). These models are widely used in chemical engineering for vapor-liquid and liquid-liquid equilibria and provide a semi-predictive way to handle large families of organic solutes. As the cryobiology field moves toward rational design of multi-component CPA cocktails (including natural deep eutectic solvents and polymer-rich formulations), such models offer a path to predictive screening of candidate mixtures without the need to commit to extensive experimental testing.

2.1.3 Phase equilibria

Armed with these solution models of the chemical potential, we are now empowered to mathematically predict or describe the melting points, solubilities, eutectics, and other cryopreservation-relevant equilibria of aqueous cryoprotectant solutions. We will describe two simple methods by which to achieve this.

First, we may simply calculate the chemical potential of water in solution at a desired concentration, using any of the theories above, compare it to the chemical potential of ice drawn from any robust equation of state [5], and identify the conditions under which the two are equal. **Fig. 1a** shows this method for solutions of NaCl in water, using the SeaFreeze equation of state for the chemical potential of water in ice-Ih and aqueous NaCl solutions, with the corresponding liquidus curve shown in **Fig. 1b**. **Fig. 1c,d** show the predicted liquidus curves for binary solutions of glycerol or sucrose computed using the ideal, size-dependent ideal, and osmotic-virial equations.

A more compact route to determining the phase coexistence exploits the Gibbs-Helmholtz relation, which for a pure substance is written as

$$\frac{\partial}{\partial T} \left(\frac{\mu}{RT} \right)_p = -\frac{h}{RT^2} \quad (18)$$

and for the difference between liquid and solid phases as

$$\frac{\partial}{\partial T} \left(\frac{\Delta\mu_{\text{liquid-solid}}^0}{RT} \right)_p = -\frac{\Delta h_{\text{liquid-solid}}^0}{RT^2} \quad (19)$$

where $\Delta H_{\text{liquid-solid}}^0$ is the enthalpy of fusion of pure water (i.e., ΔH_f^0). At the melting point of a solution, the liquid is in equilibrium with (practically) pure ice, so

$$\mu_w^{0,\text{ice}}(T_m) = \mu_{w,\text{aq}}(T_m, a_w) = \mu_w^{0,\text{liq}}(T_m) - \pi R T_m M_w \quad (20)$$

Hence

$$\pi = \frac{1}{M_w R} \int_{T_m}^{T_m^0} \frac{\Delta H_f^0}{T^2} dT \quad (21)$$

At the melting point, the enthalpy and entropy are related by $\Delta H_f^0 = T \Delta S_f^0$, and so the entropy of fusion can be substituted in the place of enthalpy in these relations. This integral form of the above expression is exact for a given $\Delta H_f^0(T)$, but the temperature dependence of enthalpies may not always be known. To a first-order approximation, the enthalpy of fusion may be assumed independent of temperature ($\Delta H_f^0(T) \approx \Delta H_f^0(T_m)$) yielding the 0th-order Gibbs-Helmholtz liquidus relation:

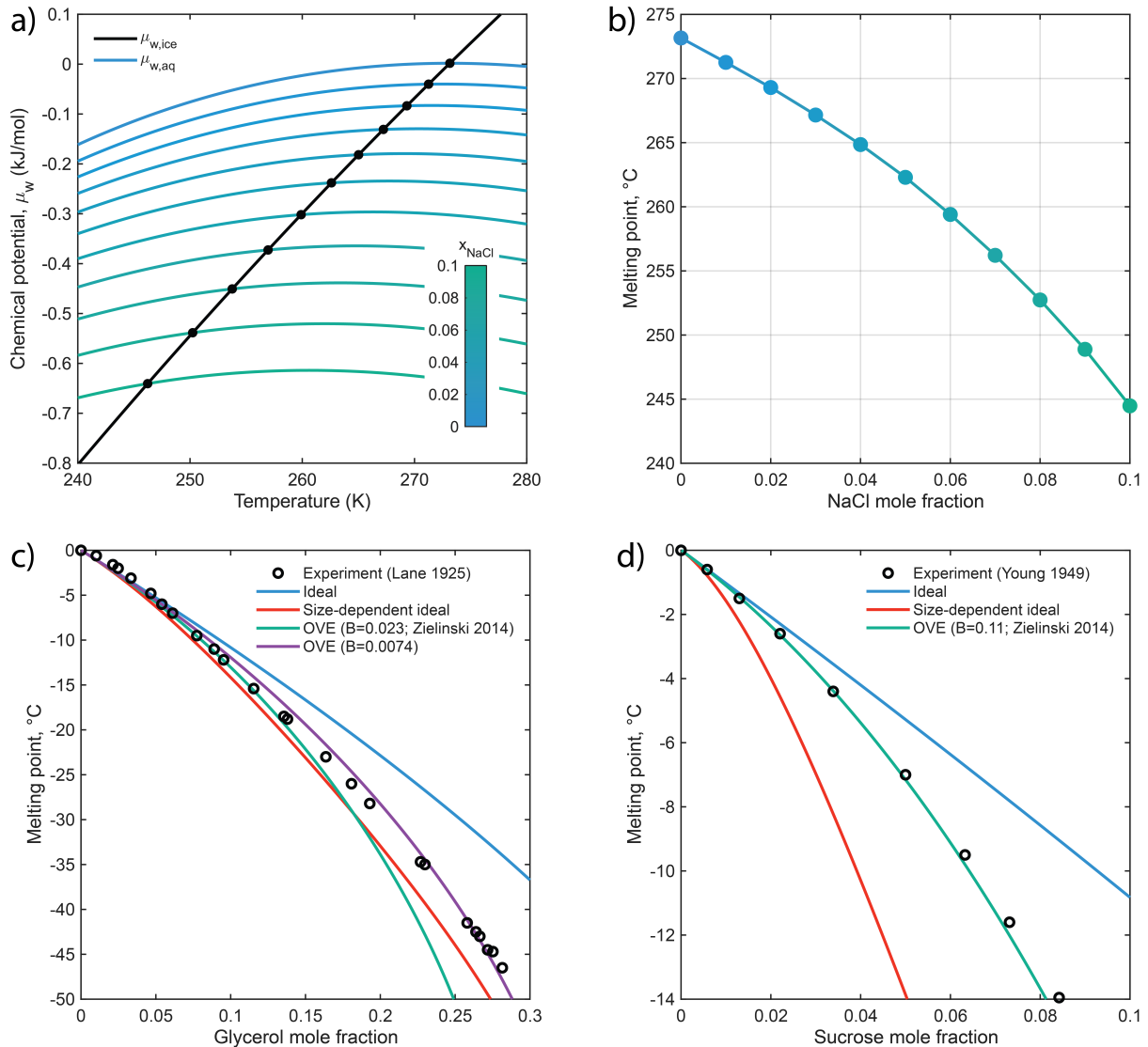


Fig. 1. Equilibrium melting points. a) Chemical potential of water in solution with NaCl and in ice as a function of temperature and b) corresponding liquidus curve. Intersections of the ice and water curves denote the coexistence temperature (i.e., T_m). Melting point as a function of mole fraction for a typical b) permeating solute (glycerol) and c) non-permeating solute (sucrose).

$$\pi \approx \frac{\Delta H_f^0}{M_w R} \left(\frac{1}{T_m} - \frac{1}{T_m^0} \right) \quad (22)$$

This may also be rearranged to provide a closed-form expression for the dependence of the coexistence temperature on the osmolality (or solvent activity in the more general case):

$$T_m \approx \left(\frac{1}{T_m^0} + \frac{\pi R M_w}{\Delta H_f^0} \right)^{-1} \quad (23)$$

Due to the wide availability of tabulated enthalpy of fusion values, the 0th-order Gibbs-Helmholtz relation is particularly useful. A more accurate (though data-intensive) description involves a first-order expansion of the enthalpy of fusion via the heat capacity ($\Delta H_f(T) \approx \Delta H_f^0 + (T - T_m^0) \Delta C_p^0$), yielding

$$\pi \approx \frac{\Delta H_f^0}{M_w R} \left(\frac{1}{T_m} - \frac{1}{T_m^0} \right) + \frac{\Delta C_{p,f}^0}{M_w} \left(\frac{T_m^0}{T_m} - \ln \left(\frac{T_m^0}{T_m} \right) - 1 \right) \quad (24)$$

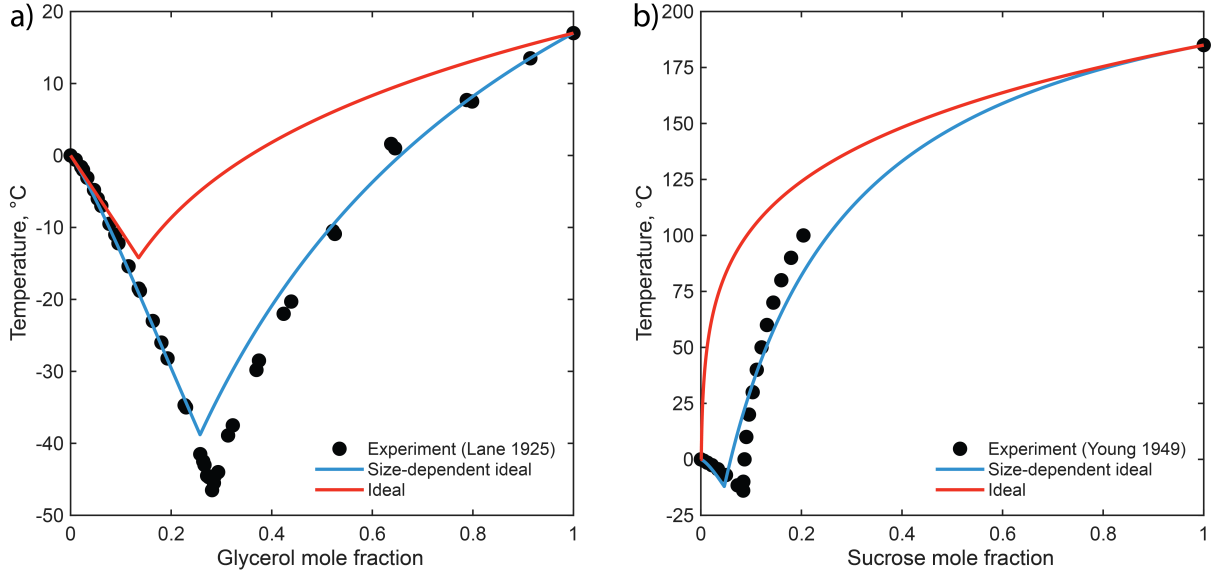


Fig. 2. Eutectic phase diagrams for binary aqueous solutions generated via size-dependent and ideal predictive models. Experimental data from the literature is shown in gray markers for a) glycerol and b) sucrose. Both models require only pure component properties, and do not require empirical information on the solution itself.

From Equation 22 we can also derive the cryoscopic constant for water, $K_f = -1.86$ K per osmole/kg, which is a proportionality constant relating the melting point depression (relative to pure water) to the solution osmolality:

$$K_f = \frac{RT_{m,0}^2 M_w}{\Delta H_f^0} \approx \frac{\Delta T_m}{\pi} \quad (25)$$

With these relations it is readily possible to compute the melting point of a solution given the osmolality (or the osmolality given the melting point). The 0th-order approximation remains accurate to within 1 °C down to -28 °C and both the first-order approximation and cryoscopic ratio down to roughly -52 °C.

One exemplary application of the first-order Gibbs-Helmholtz relation is the computation of eutectic phase diagrams (liquidus and solidus curves inclusive) using only pure component data (ΔH_f^0 and T_m^0). Alliston, et al.⁶ recently reported that the size-dependent 0th-order Gibbs-Helmholtz relation provides remarkably accurate predictions of binary eutectic phase transitions in cryobiologically relevant binary solutions. Examples for glycerol and sucrose are depicted in **Fig. 2**.

2.1.4 Isochoric phase equilibrium

Thus far much of the discussion has considered systems under isobaric conditions—those in which the system is in contact with a pressure reservoir such as the atmosphere, and for which volume is able to freely vary. In isochoric (constant volume or confined) systems [18, 19], the *volume* of the system is controlled instead, and the *pressure* is free to vary. This thermodynamic situation arises when a sample is cryopreserved within a rigid, hermetically sealed container absent air (or any bulk gas phase), referred to in recent literature as an isochoric chamber. Under isochoric conditions, the natural thermodynamic variables are $\{T, V, x\}$, and the according thermodynamic potential describing the system is the Helmholtz free energy. Thus, the equilibrium conditions become

$$\mu_{w,aq} = \mu_{w,ice} : \quad \mu_{w,aq}^v - \bar{v}_{w,aq} \left(\frac{\partial \mu_{w,aq}^v}{\partial \bar{v}_{w,aq}} \right)_{T,x} = \mu_{w,ice}^v - \bar{v}_{w,ice} \left(\frac{\partial \mu_{w,ice}^v}{\partial \bar{v}_{w,ice}} \right)_{T,x} \quad (26)$$

$$P_{aq} = P_{ice} : \quad \left(\frac{\partial \mu_{w,aq}^v}{\partial \bar{v}_{w,aq}} \right)_{T,x} = \left(\frac{\partial \mu_{w,ice}^v}{\partial \bar{v}_{w,ice}} \right)_{T,x} \quad (27)$$

$$T_{aq} = T_{ice} \quad (28)$$

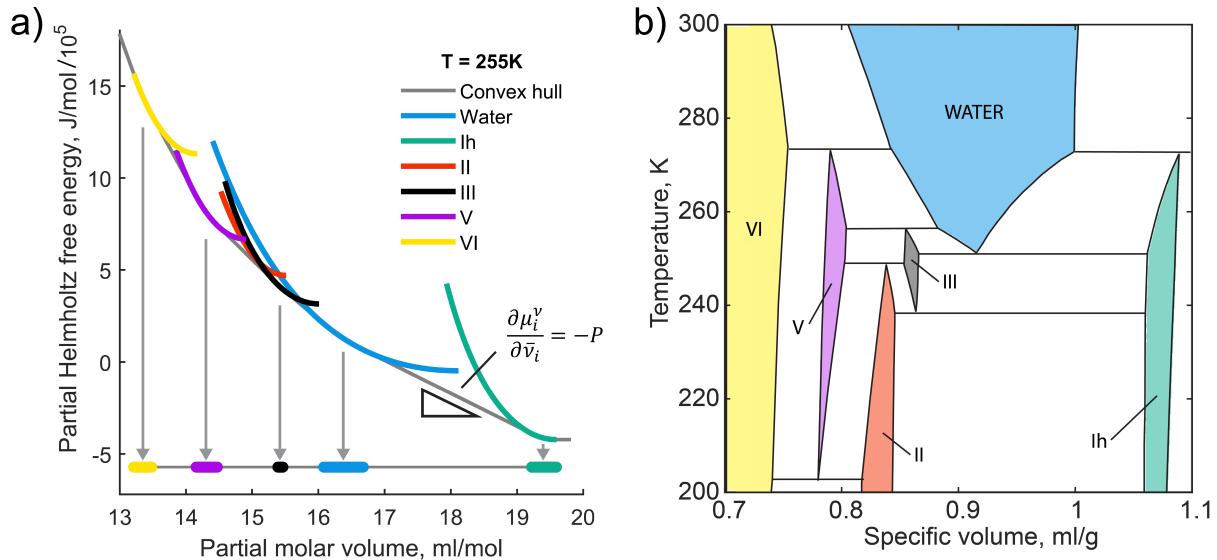


Fig. 3. Isochoric equilibrium: a) Convex hull construction for determination of phase equilibria. b) Isochoric T – v phase diagram for pure water. Adapted with permission from Consiglio et al. [19].

where \bar{v} is the partial molar volume and μ_w^V is the partial molar Helmholtz free energy. These equalities are supplemented by the condition that the sum of the volumes of individual phases must equal the system volume (i.e., $v_{\text{sys}} = (1 - f_{\text{ice}})v_{\text{aq}} + f_{\text{ice}}v_{\text{ice}}$, with f_{ice} as the volumetric phase fraction of ice).

Fig. 3a shows a schematic convex-hull construction [20] of the Helmholtz free energy curves for several phases of water under isochoric conditions, and **Fig. 3b** shows the resulting isochoric T – v phase diagram for pure water. For many specific volumes, cooling at fixed v necessarily drives the system into a two-phase (ice + liquid) coexistence region, even when the corresponding isobaric path would remain single-phase. Practically, this enables preservation of biological matter at sub-0 °C temperatures in the portion of the isochoric system that remains liquid, thereby protecting it from ice formation. For a thorough review of both the theory and practice of isochoric cryopreservation, we refer the reader to Consiglio et al. [19].

2.1.5 Phase fraction and the lever rule

In addition to the temperature at which ice may begin to form, cryobiologists are also often interested in the *amount* of ice that will form at a given temperature. For a binary solution at constant pressure, a typical T – x phase diagram produces a two-phase liquid–ice region beneath the liquidus curve. A system with overall solute mole fraction x_0 cooled to a temperature T such that the coordinates $[T, x_0]$ are inside this two-phase region (**Fig. 4a**) will separate into distinct phases with liquid and solid solute concentrations x_{liquid} and x_{solid} . Conservation of mass gives:

$$x_0 = f_{\text{liquid}}x_{\text{liquid}} + (1 - f_{\text{liquid}})x_{\text{solid}} \quad (29)$$

where f_{liquid} is the phase fraction that remains liquid (in units that match the concentration, be they weight fraction, volume fraction, mol fraction, etc.). In aqueous solutions, the solute concentration in the solid ice phase is typically taken as $x_{\text{solid}} \approx 0$, because ice rejects nearly all solutes. As such, the unfrozen phase fraction f_{liquid} for aqueous solutions simplifies to

$$f_{\text{liquid}} = \frac{x_0}{x_{\text{liq}}} \quad (30)$$

As depicted in **Fig. 4a**, the value of x_{liq} is given by the concentration coordinate of the liquidus curve at the sub-freezing temperature T , and this same expression may be derived by graphical examination of the phase diagram, using what is commonly referred to as the “lever rule”.

In **Fig. 4b** we show the unfrozen (liquid) phase fraction f_{liquid} versus temperature for water-DMSO solutions at various starting DMSO concentrations x_0 . For small starting x_0 , a significant fraction of the system quickly transforms to ice as the temperature falls below the liquidus curve, but the rate-of-change

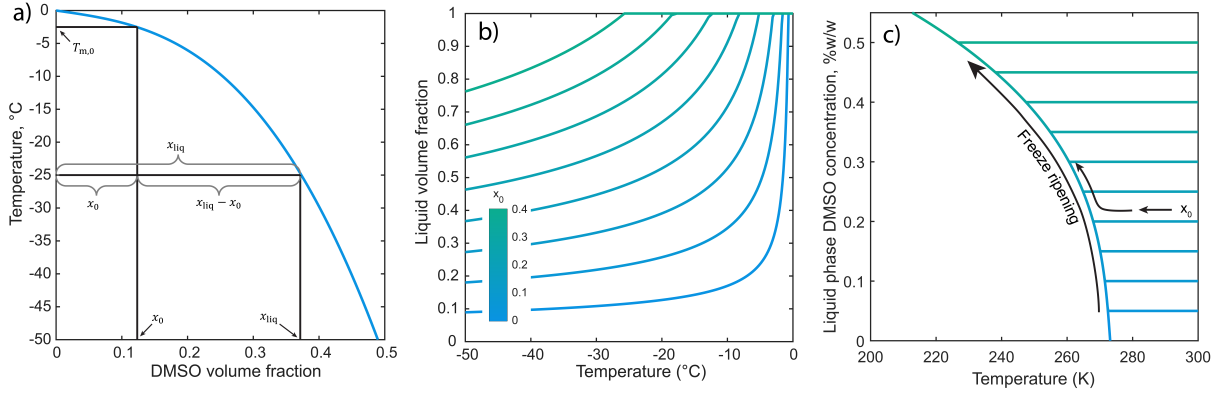


Fig. 4. Isobaric Ice-liquid phase fractions and solute ripening processes. a) Construction of the lever rule for a binary solution T-x phase diagram, which enables calculation of the fraction of the system that remains in the frozen or unfrozen state at a given temperature. b) Unfrozen phase fraction versus temperature for various starting concentrations of DMSO in a water-DMSO solution. c) According concentration of the liquid phase during progressive freezing, for the same starting concentrations indicated by the color bar in panel (b).

of this fraction with temperature decays continuously as deeper temperatures are reached. This behavior is explained by, **Fig. 4c**, which shows the corresponding liquid-phase concentration $x_{liquid}(T)$, and illustrates how solute “ripening” from rejection by the solid phase intensifies as freezing progresses. In classical slow-freezing cryopreservation protocols, this progressive concentration of the remaining liquid is deliberately exploited: as extracellular ice forms and solutes are rejected, the external solution becomes more concentrated, drawing water osmotically out of cells and thereby reducing intracellular ice formation. When carried too far, however, the same process leads to extreme extracellular solute concentrations and osmotic stresses, producing the “solution effects” injury central to Mazur’s two-factor hypothesis of freezing damage [21].

In an isochoric system filled with pure water, the same logic applies, but the conserved quantity is specific volume rather than composition. For a given temperature T and total system specific volume v_{sys} lying inside the two-phase dome of the isochoric $T-v$ diagram, the coexisting liquid and solid phases have specific volumes v_{liquid} and v_{solid} . Conservation of volume yields

$$v_{sys} = f_{liquid}v_{liquid} + (1 - f_{liquid})v_{solid} \quad (31)$$

So that

$$f_{liquid} = \frac{v_{solid} - v_{sys}}{v_{solid} - v_{liquid}} \quad (32)$$

Fig. 5 (isochoric lever rule) illustrates this construction graphically: **Fig. 5a** shows the isochoric lever rule on a specific-volume diagram, and **Fig. 5b** shows the resulting liquid fraction as a function of temperature for several choices of total specific volume. In practice, the specific volume of an isochoric system is set when the chamber is sealed—typically at 5–10 °C, giving $v_0 \approx 1$ mL/g. Other specific volumes can be accessed by deliberately including a vapor space (increasing v_0) or by compressing the system with a piston (decreasing v_0). If the liquid filling the isochoric chamber is not pure water, but instead an aqueous solution, a 3-dimensional lever rule may be devised which conserves both phase volume *and* phase concentration.

In summary, the tools of multi-phase equilibrium thermodynamics—regardless of the specific theories used to compute chemical potential—allow us to map solution composition (and, in isochoric systems, specific volume) to melting points, eutectics, and equilibrium phase fractions. These maps in turn underpin the thermodynamic design and analysis of equilibrium-dominated cryopreservation strategies such as liquidus tracking, partial freezing, and isochoric freezing, and they set the backdrop against which kinetic and transport phenomena act in more complex protocols.

2.2 Ice nucleation and growth

Having established how equilibrium thermodynamics dictates the conditions under which liquid water and ice can coexist, we next consider how a system *transitions* between these phases. In practice, freezing proceeds by the stochastic formation of microscopic ice nuclei, followed by their subsequent growth.

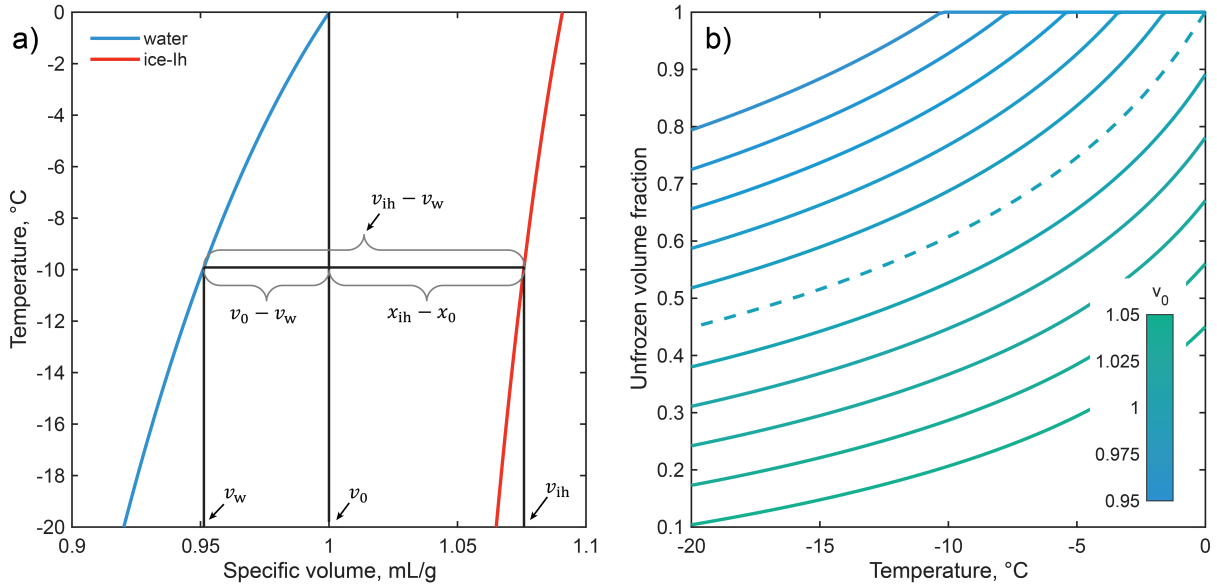


Fig. 5. Isochoric ice-liquid phase fractions for pure water. a) Construction of the isochoric lever rule from the water/ice Ih temperature-specific volume phase diagram derived by Powell-Palm et al. [20]. b) Fraction of isochoric system that remains liquid during isochoric freezing as a function of system specific volume.

The standard framework for describing this process is classical nucleation theory (CNT), which links the statistics of ice nucleation directly to the underlying solution thermodynamics and interfacial properties. We will here review salient aspects of this theory, emphasizing both its practical applications in cryopreservation and its connection to equilibrium thermodynamics.

2.2.1 The nucleation barrier

The formative relations of CNT are derived by considering the change in energy in a system between a first state in which the entire system is liquid and a second state in which a nucleus (a stable cluster of molecules) of a solid phase (here ice) has emerged (Fig. 6).

Assuming the volume of the system is much larger than that occupied by the emerging solid, the free energy of these two states may then be written as:

$$G_1 = \mu_{w,aq}^1 N_{w,aq}^1 + \mu_{s,aq}^1 N_{s,aq}^1 \quad (33)$$

$$G_2 = \mu_{w,aq}^2 N_{w,aq}^2 + \mu_{s,aq}^2 N_{s,aq}^2 + \mu_{w,ice}^2 N_{w,ice}^2 + 4\pi R^2 \sigma_{iw} \quad (34)$$

In State 1, $\mu_{w,aq}^1 N_{w,aq}^1$ gives the free energy of bulk liquid water in solution, and $\mu_{s,aq}^1 N_{s,aq}^1$ gives that of the solute. In State 2, the free energy of the bulk incipient ice phase is further given by $\mu_{w,ice}^2 N_{w,ice}^2$.

The last term in G_2 , which encodes the most critical phenomenological insight provided by CNT, gives the *surface energy* of the ice nucleus, or the energetic and entropic toll exacted upon the system in order to host two phases where previously there was one. The proportionality constant of this energy is given by the *liquid-ice interfacial free energy* σ_{iw} , which describes the energy required per unit surface area of the ice nucleus to bound it from the liquid phase.

Again, assuming a small initial ice nucleus relative to the volume of the system, we may take $\mu_{w,aq}^1 \approx \mu_{w,aq}^2$ and $\mu_{s,aq}^1 \approx \mu_{s,aq}^2$. It is customary (if arbitrary) also to treat the emerging ice nucleus as spherical, with volume $V = \frac{4}{3}\pi R^3 = v_{ice}N$ and surface area $SA = 4\pi R^2 = (36\pi)^{1/3}V^{2/3}$. Armed with these assumptions, we may now write the *difference* in free energy upon spontaneous formation of an ice nucleus (the difference between States 1 and 2) as:

$$\Delta G_{nuc} = G_2 - G_1 = \frac{4}{3}\pi R^3 \left(\frac{\Delta\mu}{v_{ice}} \right) + 4\pi R^2 \sigma_{iw} \quad (35)$$

Critically, the two terms comprising this equation exist in competition. Given the lower free energy of solid ice relative to liquid water at any sub-melting temperature, the first term (often referred to

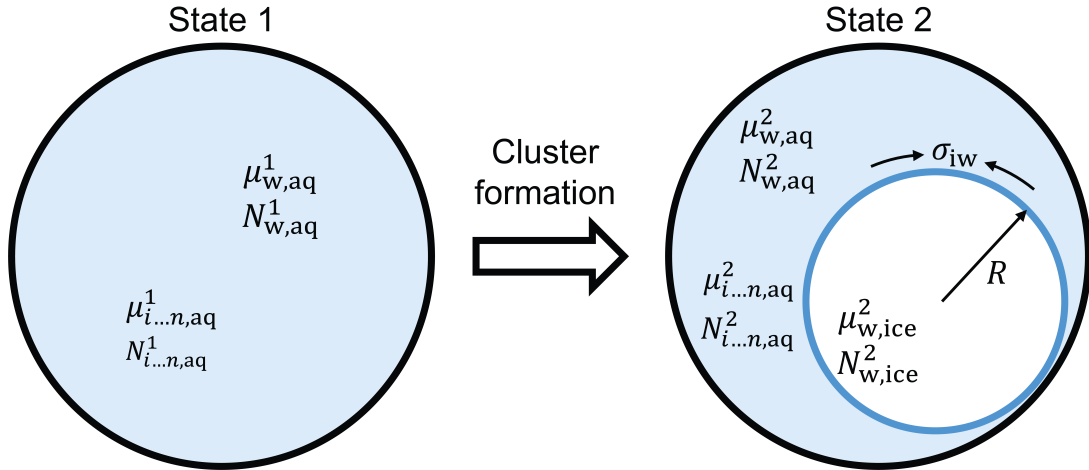


Fig. 6. Conceptual illustration of the change in free energy upon formation of a solid nucleus from a supercooled liquid.

as the “bulk” term) is negative, and scales with the *volume* of the growing ice phase, representing the spontaneous drive of the system to convert to the more stable phase. Meanwhile, because the segregation of an ordered crystalline phase from the disordered liquid must necessarily *reduce* the entropy of the system, the second term (often referred to as the “surface” term) must accordingly be positive, *increasing* the free energy of the system and scaling with the *surface area* of the nucleus.

It is this surface-versus-volume competition that belies the nature of nucleation as an activated stochastic process, and gives the nucleation free energy difference ΔG_{nuc} its characteristic maximum (**Fig. 7**), referred to as the nucleation barrier ΔG_{nuc}^* :

$$\Delta G_{\text{nuc}}^* = \Delta G_{\text{nuc}} \Big|_{\frac{\partial \Delta G_{\text{nuc}}}{\partial N} = 0} = \frac{16\pi\sigma_{\text{iw}}^3 v_{\text{ice}}^2}{3\Delta\mu^2} \quad (36)$$

The random thermal motion of water molecules in the solution causes the system to fluctuate and sample a variety of possible configurations, which may include clusters of water molecules arranged in the cubic or tetrahedral structures defining ice Ic or Ih. The cluster size corresponding to ΔG_{nuc}^* gives “critical” cluster size (or “critical radius” if not discretizing by number of molecules), and the fate of any spontaneously assembled cluster of molecules is prescribed by its relation to this critical size.

Any smaller (“sub-critical”) cluster, once assembled by a random fluctuation, in order to then decrease its free energy and march towards equilibrium, will be compelled to dissolve, as recruitment of additional molecules would *increase* its free energy in defiance of the 2nd Law of Thermodynamics. Equally, any cluster produced by random fluctuation that is *larger* than the critical size will be compelled to *grow* continuously until equilibrium is reached, initiating bulk phase crystallization or freezing. It is this critical or supra-critical cluster that we refer to as a stable ice *nucleus*.

2.2.2 The nucleation rate

The nucleation barrier ΔG_{nuc}^* connects the process of ice nucleation to the underlying bulk thermodynamics of the aqueous solution, via the chemical potential difference $\Delta\mu$ between solid ice and liquid water in solution, and to the surface thermodynamics of the solution via σ_{iw} . In isolation, this barrier provides only relative or trend-level insight into the ease or difficulty of ice nucleation in a given solution at a given temperature. To valorize this information, we may then incorporate this barrier as a rate constant in a probabilistic description of a stochastic activated process (i.e. one driven by random molecular fluctuation), yielding a *nucleation rate* J [nuclei formed per m³ per second]:

$$J = J_0 \exp\left(-\frac{\Delta G_{\text{nuc}}^*}{k_{\text{B}}T}\right) \quad (37)$$

The nucleation rate J is comprised of two general terms, the exponential driver of the process $\exp\left(-\frac{\Delta G_{\text{nuc}}^*}{k_{\text{B}}T}\right)$ and the pre-factor $J_0 = \frac{Zf^*}{v_0}$. We refer to the exponential portion as the thermodynamic term, describing a simple classical Arrhenius-style kinetic process for which the characteristic constant

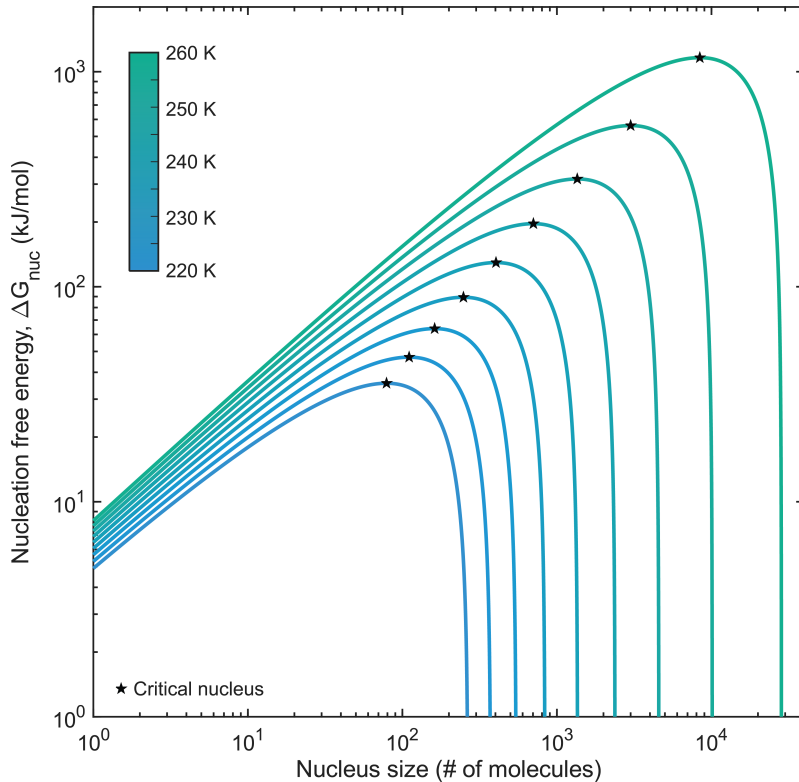


Fig. 7. Free energy change upon nucleation versus ice cluster size for pure water at various temperatures. The nucleation barrier for each temperature is marked by a black star. Consistent with expectation, the nucleation barrier grows exponentially higher as the equilibrium melting temperature is approached, at which point it reaches singularity due to the chemical potential difference in the denominator of Equation 36 reaching zero.

is the nucleation barrier. This term represents the probability of a token stochastic fluctuation achieving the critical cluster size. We refer to the pre-factor J_0 as the kinetic term, which in turn captures the aspects of the nucleation process that are not captured by connections to bulk thermodynamics, but instead by microscale transport processes. Here, f^* gives the attachment frequency factor, which describes the probability of a given cluster recruiting additional water molecules based on barriers to diffusion in the solution, the Zeldovich factor Z gives the likelihood that a nucleus of precisely the critical size will either dissolve or grow (“roll” to the left or right of the maximum of the nucleation free energy curve in **Fig. 7**), and v_0 is the molecular volume of ice.

The nucleation rate may thus be thought of as a constant competition between the kinetic and diffusive terms. At higher temperatures, where (for cryobiological applications) solution viscosity is typically relatively low (and thus diffusivity relatively high), the nucleation process is dominated by the kinetic term, and therefore the underlying solution thermodynamics. As the temperature decreases towards the glass transition and the viscosity increases, however, the diffusive term will eventually come to dominate, preventing the recruitment of new molecules to a potentially critical nucleus, and thereby hindering the nucleation process. This transition of dominance between the two terms is embodied in temperature-time-transformation curves, which show that for any material, there exists a maximum in nucleation rate located at some temperature between that of melting and that of glass transition [22].

The rate equation J further reveals the critical role of the surface effects in the nucleation process; J is an exponential function of the water-ice interfacial free energy σ_{iw} to the third power, introducing extraordinary sensitivity to this parameter. For example, assuming typical values of J_0 for pure water [23], a 10% change in the value of σ_{iw} can change the nucleation rate by >10 orders of magnitude. This sensitivity renders accurate prediction of the precise nucleation rate difficult, and recent studies have suggested that targeting this parameter via molecular or solution design strategies may present a potent engineering lever with which to control cryobiological ice nucleation [9].

2.2.3 Growth after nucleation

After a critical ice nucleus forms, bulk crystallization will proceed. For pure water, the growth rate of ice in this phase is often modeled using the Wilson-Frenkel relation [24]:

$$U(T) = \frac{D}{a} \left[1 - \exp \left(-\frac{|\Delta\mu|}{RT} \right) \right] \quad (38)$$

Wherein D is the water diffusivity, $\Delta\mu$ is the chemical potential difference between water in the liquid phase and ice, and a is characteristic length often specified as the interfacial thickness or water molecular mean free path length. Like the nucleation rate, at small supercoolings, U is limited by the thermodynamic driving force (via $\Delta\mu$), whereas at deeper supercoolings it is limited by diffusion (via D). For cellular systems, the interplay between growth kinetics and cellular water transport rate controls whether ice remains extracellular or propagates into the intracellular space [25].

For aqueous solutions, the same basic Wilson-Frenkel concept can be applied if we replace the pure-water driving force with the chemical-potential difference of water between the solid and the local solution at the interface. In local equilibrium models, $\mu_{w,ice}(T, p)$ is set equal to $\mu_{w,liq}(T, p, x_i)$ along the interface, where x_i is the interfacial solute mole fraction. As ice advances and rejects solute into the liquid, x_i departs from the bulk composition x_∞ , and a solute-enriched boundary layer develops in front of the interface. The resulting local freezing-point depression reduces $\Delta\mu$ and progressively slows growth, even at fixed ambient temperature.

Mathematically, sharp-interface models treat growth in solutions by coupling the interface-kinetic relation to conservation laws for heat and solute transport. In a one-dimensional binary solution, the solute concentration $c(z, t)$ obeys a diffusion equation ahead of a moving interface $z = s(t)$, together with a Stefan condition $D \frac{\partial c}{\partial z} \big|_{z=s^+} = V_n (c_l - c_s)$ that enforces solute balance at the front (here V_n is the interface-normal velocity and c_l and c_s are the solute concentrations in the liquid and solid). When the solid phase excludes solute (typically $c_s \approx 0$ for ice), this boundary condition ensures that growth is accompanied by a concentrated liquid layer whose thickness and composition are controlled by the competition between interface motion (V_n) and diffusion (D). In the diffusion-limited regime V_n is set by how rapidly this boundary layer can be relaxed, whereas in the interface-limited regime V_n is controlled primarily by attachment kinetics at the ice surface.

A convenient way to summarize these regimes is to view the observed growth rate as the harmonic mean of an interface-limited velocity V_{kin} and a diffusion-limited velocity V_{diff} , i.e., $V_n^{-1} \approx V_{kin}^{-1} + V_{diff}^{-1}$. V_{kin} can be estimated from Wilson-Frenkel-type expressions that scale with the chemical-potential driving force, while V_{diff} scales with D times the ratio of the available undercooling to the liquidus slope and the characteristic diffusion length ahead of the interface. In concentrated CPA cocktails near the glass transition, D becomes so small that V_{diff} effectively vanishes and growth is arrested even though the thermodynamic driving force remains substantial. In moderately concentrated solutions at higher temperatures, by contrast, D is large enough that interface kinetics still play a significant role and growth can proceed rapidly once nucleation has occurred.

Beyond one-dimensional planar growth, solute interactions with the advancing front also determine the morphology of the ice phase. When the solute boundary layer is sufficiently strong that the local liquidus temperature ahead of the interface drops faster than the actual temperature field, a region of so-called constitutional supercooling is created. Under these conditions small perturbations of the interface are amplified rather than damped, leading to cellular or dendritic ice structures instead of a smooth front. In cryobiological samples this translates into complex networks of extracellular ice that can mechanically entrap cells and produce highly non-uniform solute distributions, further complicating subsequent growth and warming behavior.

After the initial growth stage, ice microstructure continues to evolve even at fixed temperature through recrystallization. In broad terms, recrystallization is a curvature-driven coarsening process in which larger crystals grow at the expense of smaller ones. Because the equilibrium melting temperature of a curved interface depends on its radius via a Gibbs-Thomson relation, small, highly curved crystals have a slightly higher chemical potential and lower melting temperature than large, gently curved ones. This difference in chemical potential drives net mass transfer from small to large crystals through melting-recrystallization cycles, leading over time to a reduction in total grain-boundary area and a progressive increase in the characteristic crystal size.

Classical Ostwald ripening theories describe this coarsening in terms of diffusion-limited transport of water through an intervening liquid or glassy matrix, predicting a characteristic length scale that grows as a power-law in time (often $t^{1/3}$ for simple systems). In CPA-rich, partially vitrified, or highly

viscous solutions relevant to cryopreservation, the effective diffusivity is strongly temperature dependent, so that recrystallization is negligible at deep cryogenic temperatures but can proceed rapidly when the sample is held or passes slowly through warmer sub-zero ranges (for example, between roughly $-20\text{ }^{\circ}\text{C}$ and $-5\text{ }^{\circ}\text{C}$). For cells and tissues, such coarsening can be particularly damaging, because it transforms initially fine-grained, relatively benign ice networks into larger crystals that can disrupt membranes and extracellular matrices.

One of the major rationales for adding so-called ice recrystallization inhibitors (IRIs) to cryopreservation media is precisely to slow or arrest this curvature-driven coarsening. Natural anti-freeze proteins and glycoproteins, as well as synthetic polymers such as certain poly(vinyl alcohols) and related ampholytes, can adsorb selectively to particular ice crystal faces, pinning step motion and reducing the surface mobility needed for grain-boundary migration [26–29]. In continuum terms, these additives effectively reduce the kinetic coefficient associated with interface motion without necessarily changing the underlying thermodynamic driving force. The result is a dramatic suppression of recrystallization over experimentally relevant time scales, which can preserve a fine-grained ice morphology during storage and through slow warming, thereby mitigating mechanical and osmotic injury even when some ice is present.

2.2.4 Heterogeneous nucleation

In practical cryopreservation, ice almost never nucleates homogeneously in the bulk solution. Instead, nucleation is overwhelmingly *heterogeneous*: it occurs on foreign surfaces such as container walls, extracellular matrices, cellular membranes, or deliberately added ice nucleating agents (INAs). From the perspective of classical nucleation theory, these surfaces lower the free-energy barrier for forming a critical nucleus, thereby shortening the induction time and raising the probability of nucleation at comparatively mild supercooling [30].

The simplest and most widely used description of heterogeneous nucleation is the spherical-cap model. Here, the ice embryo is assumed to form as a cap on an ideal, flat substrate rather than as a full sphere in the bulk liquid. The geometry is characterized by a contact angle θ between the ice, the liquid, and the substrate. Under this construction, the free-energy barrier for heterogeneous nucleation can be written as a simple multiplicative correction to the homogeneous barrier [30],

$$\Delta G_{\text{het}}^* = f(\theta) \Delta G_{\text{hom}}^* \quad (39)$$

where ΔG_{hom}^* is the barrier derived in the homogeneous case and $f(\theta)$ is the geometric factor that accounts for the reduced nucleus volume and surface area. For $\theta \rightarrow 180^\circ$ (perfectly non-wetting substrate), ($f(\theta) \rightarrow 1$) and the surface has no effect. For $\theta \rightarrow 0^\circ$ (perfectly wetting substrate), ($f(\theta) \rightarrow 0$) and the barrier may be reduced by many orders of magnitude. Because the nucleation rate depends exponentially on $\Delta G^*/k_B T$, even modest changes in θ (and thus in f) can transform nucleation from effectively impossible to nearly instantaneous under otherwise identical conditions.

To connect this barrier reduction to observable nucleation rates, we may simply replace ΔG_{hom}^* with ΔG_{het}^* in the CNT rate expression, yielding a heterogeneous nucleation rate [30]

$$J_{\text{het}} = J_0 \exp \left(-\frac{f(\theta) \Delta G_{\text{hom}}^*}{k_B T} \right) \quad (40)$$

where J_0 is again the kinetic prefactor. In the immersion mode most relevant to cryobiology, nucleation is assumed to occur on active sites that are fully wetted by the solution (e.g. a nucleator particle or a patch of the container surface immersed in the liquid). The total nucleation rate is then proportional to both the site-specific rate (J_{het}) and the density (or number) of such active sites, so that both site strength (through θ or equivalent parameters) and site abundance determine the macroscopic stability of a supercooled sample.

Real cryobiological systems, however, rarely present a single, idealized contact angle, and thus are seldom adequately described by the spherical cap interpretation of heterogeneous nucleation. Instead, a given surface in contact with the liquid may host a spectrum of active sites, each characterized by its own local barrier height and kinetics. Mineral particles, polymer-coated chamber walls, proteins embedded in extracellular matrices, and bacterial ice nucleating proteins all provide distinct microenvironments for vicinal water molecules, and thus distinct effective nucleation parameters [31]. Contemporary descriptions of heterogeneous nucleation therefore supplement the geometric contact-angle model with active-site distributions, in which each site type is assigned a characteristic barrier (or contact angle) and an areal density. The observed nucleation statistics then arise from an extreme-value competition among these

sites: nucleation almost always occurs at the *most active* site present, not at a hypothetical average site (**Fig. 9c** shows family of extreme value distributions describing active site variability). This framework underlies the extreme-value statistics models increasingly used to interpret cryobiological nucleation experiments and to quantify the stability of supercooled systems [32].

An alternative but complementary view, emphasized in more recent work by Barahona [31, 33, 34], focuses less on the static contact angle and more on ice templating and the dynamics of vicinal water. In this view, an active site is one that organizes nearby water into motifs structurally compatible with ice (thereby lowering the entropic cost of forming an ordered cluster) and/or modifies the local energy landscape so as to reduce the work required to assemble a critical nucleus. Crystalline substrates whose lattice spacings closely match those of basal or prism planes of ice can act as nearly perfect templates, strongly reducing the interfacial free energy and effectively lowering ΔG^* . At the same time, adsorption of solutes or macromolecules onto the substrate can slow local water mobility, altering the kinetic prefactor, J_0 . Some authors therefore introduce an explicit *templating factor* that multiplies the homogeneous rate by a function of both geometric matching and local dynamical slowdown, rather than relying solely on a geometric $f(\theta)$. With the templating factor ζ varying between 0 (no templating) and 1 (full templating), a nucleation site-specific, surface area-normalized heterogeneous nucleation rate can be summarized as

$$J_{\text{het}} = \frac{Z f^*(\zeta)}{a_0} \exp\left(-\frac{\Delta G_{\text{het}}^*(\zeta)}{k_B T}\right) \quad (41)$$

in which $f^*(\zeta)$ is the attachment frequency factor, Z is the Zeldovich factor, a_0 is the molecular cross-sectional area of water, and $\Delta G_{\text{het}}^*(\zeta)$ is the surface-dependent nucleation barrier. This rate is plotted in **Fig. 8** below for pure water.

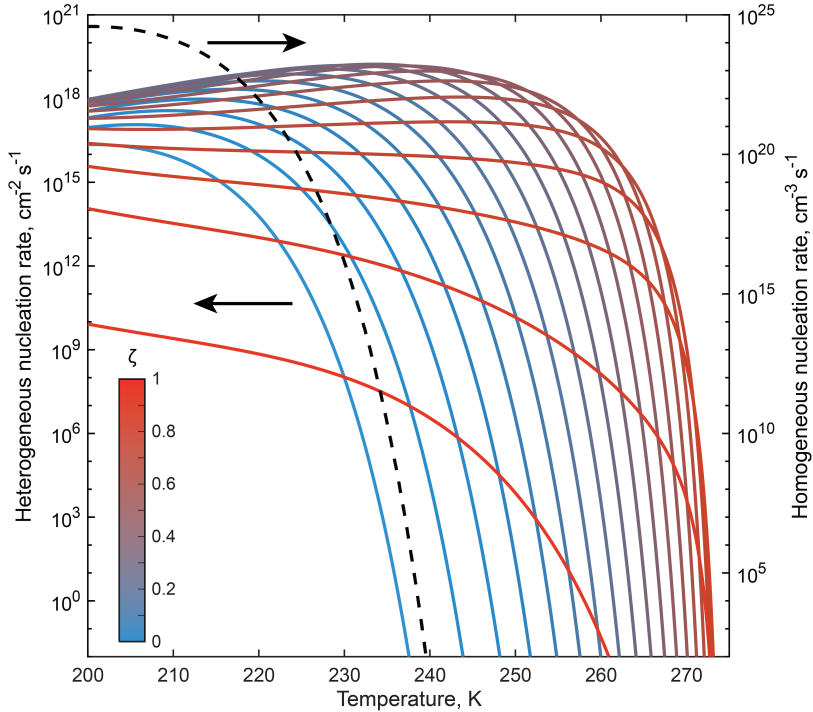


Fig. 8. Surface-scaling heterogeneous and volume-scaling homogeneous ice nucleation rates as a function of temperature. Shown for pure water and various values of Barahona's ice "templating factor" [31], which encodes the degree to which a foreign surface modifies the local free energy landscape so as to reduce the work required to assemble a critical nucleus.

From a cryobiological design standpoint, heterogeneous nucleation is both a nuisance and a tool. On one hand, unwanted active sites - including microscopic scratches or contaminants on container walls, undissolved particulates, or patches of gas-liquid interface - dramatically raise nucleation temperatures and undermine attempts to maintain supercooling or achieve vitrification. Mitigation strategies therefore focus on minimizing, passivating, or isolating such sites: polishing or coating surfaces, eliminating gas bubbles, overlaying solutions with immiscible liquids, or confining samples in smooth, rigid, air-free

isochoric chambers (see **Section 3.2**). On the other hand, for ice seeding and partial freezing protocols, the goal is, precisely to *create* highly active heterogeneous sites in carefully chosen locations (e.g. in the extracellular space or in the perfusate), so that nucleation occurs reproducibly at modest supercooling and in mechanically benign regions. Engineered ice nucleating agents, from mineral particles to synthetic macromolecules and bacterial ice nucleation proteins, can thus be seen as deliberate manipulations of the heterogeneous nucleation landscape, tuning both the barrier (via geometry and templating) and the site density to produce desired nucleation statistics.

In summary, heterogeneous nucleation extends classical nucleation theory by incorporating the effects of real surfaces and interfaces into the free-energy barrier and kinetic prefactor. As such, whether a given cryopreservation protocol succeeds in stabilizing a supercooled or vitrified state, or in achieving a well-timed ice seeding event, may depend less on the homogeneous properties of the bulk solution and more on the nature, distribution, and management of these heterogeneous nucleation sites.

2.2.5 Statistical aspects of ice nucleation

While classical nucleation theory describes nucleation as a *continuous* process in time via the nucleation rate, J , the formation of a single nucleus remains a discrete process: long, seemingly quiescent periods with no events are punctuated by individual instances of critical nucleus formation. Despite the conceptual prevalence of CNT, what the cryobiologist actually *observes* in most experiments and protocols are these discrete nucleation outcomes, e.g. “frozen” vs. “unfrozen”, recorded at particular times or temperatures. Connecting these discrete and continuous views of nucleation enables marriage of laboratory outcomes to broader kinetic understanding of the kinetic phenomena at play, and requires treating nucleation as a purely probabilistic process.

This may be achieved by use of Poisson statistics, which describe the probabilistic nature of memoryless stochastic events [35]. Within this framework, for a system at temperature T with an effective nucleation rate $J_{\text{sys}}(T)$, the expected number of nucleation events accumulated over a time interval $[0, t]$ is $J_{\text{sys}}(T) \cdot t$. Assuming that each possible nucleus forms independently, the probability of observing no nucleation events in that interval is

$$S(T, t) = \exp(-J_{\text{sys}}(T)t) \quad (42)$$

which is the survival probability of the metastable liquid. The probability of at least *one* nucleation event having occurred by time, t , is then $P(T, t) = 1 - S(T, t)$. Formally, this is the cumulative distribution function of a homogeneous Poisson process with rate J_{sys} (see example distributions in **Fig. 9a**). The corresponding probability density function for the waiting time to the first event is

$$p(T, t) = \frac{\partial P}{\partial t} = J_{\text{sys}}(T) \exp(-J_{\text{sys}}(T)t) \quad (43)$$

which is an exponential distribution. The characteristic time until nucleation (the mean waiting time, often referred to as the induction time) is therefore the average time $\langle t \rangle$:

$$t_{\text{nuc}} = \frac{1}{J_{\text{sys}}(T)} \quad (44)$$

More generally, if one wishes to guarantee that the probability of nucleation does not exceed some small failure probability p^* during a hold at temperature, T , the maximum allowable hold time is

$$t_{p^*}(T) = -\frac{\ln(1 - p^*)}{J_{\text{sys}}(T)} \quad (45)$$

For example, ($p^* = 0.01$) corresponds to a “1% risk” induction time; $p^* = 10^{-4}$ corresponds to the “one-in-ten-thousand” threshold often used in high-reliability engineering contexts. In most cryobiological experiments and protocols, however, the system is not held at a single temperature. Instead, the sample is cooled or warmed according to some protocol, so both T and J_{sys} vary with time. For a general time-dependent temperature history $T(t)$, the survival probability becomes

$$S(T(t)) = \exp\left(-\int_0^t J_{\text{sys}}(T(\tau)) d\tau\right) \quad (46)$$

This is the defining form of a non-homogeneous Poisson process. A particularly important special case for cryopreservation is constant-rate cooling. If the system is cooled from the equilibrium melting point,

T_m , at a constant rate, $R = |dT/dt|$, then time and temperature are related by $T(t) = T_m - Rt$, and the integral in the survival function can be re-expressed as an integral over temperature:

$$S_{CCR}(T) = \exp \left(-\frac{1}{R} \int_{T_m}^T J_{sys}(\theta) d\theta \right) \quad (47)$$

This is the non-homogeneous Poisson distribution in temperature, used in constant-cooling-rate experiments to extract nucleation rates from distributions of observed freezing temperatures. Differentiating with respect to temperature yields the probability density for nucleation to occur at temperature, T :

$$p_{CCR}(T) = \frac{\partial P_{CCR}}{\partial T} = \frac{J_{sys}(T)}{R} \exp \left(-\frac{1}{R} \int_{T_m}^T J_{sys}(\theta) d\theta \right) \quad (48)$$

An example cumulative distribution function and probability density function are shown in **Fig. 9b**. The characteristic nucleation temperature, T_{nuc} , can then be defined in several equivalent ways; for example as the mean of this distribution,

$$T_{nuc} = \int_0^{T_m} T p_{CCR}(T) dT \quad (49)$$

or, more practically, as its mode or median. In systems where J_{sys} varies extremely rapidly with undercooling (as is typical in CNT), $p_{CCR}(T)$ becomes sharply peaked, so that the “nucleation temperature” is very well-defined even though the underlying process is stochastic.

Two additional features of the Poisson description are particularly important for cryobiology. Firstly, in the simplest homogeneous case, the system nucleation rate is proportional to the system volume, so larger samples have proportionally higher nucleation rates and correspondingly shorter induction times. This makes it much easier to maintain deep supercooling or vitrification in droplets or thin films than in organs or large tissues, even if the underlying solution thermodynamics and interfacial properties are identical. More refined models replace the single volume, V , with a sum over compartments (e.g. intracellular vs. extracellular, or separate regions of an organ), each with its own local J and effective volume.

Secondly, in heterogeneous nucleation, the system often contains a spectrum of active sites, each with its own local nucleation rate $J_i(T)$. If each site is modeled as an independent Poisson process, the system-level survival probability is product of each independent survival probability, and the system level nucleation rate is a sum of the individual active site nucleation rates. When the J_i span many orders of magnitude, nucleation almost always occurs at the single most active site present, making the observed distribution of induction times or nucleation temperatures an extreme-value statistic of the underlying site population rather than a simple reflection of an average rate. This is the basis for active-site and extreme-value models that infer the strength and abundance of heterogeneous nucleation sites from experimental nucleation statistics in supercooled cryobiological systems [32].

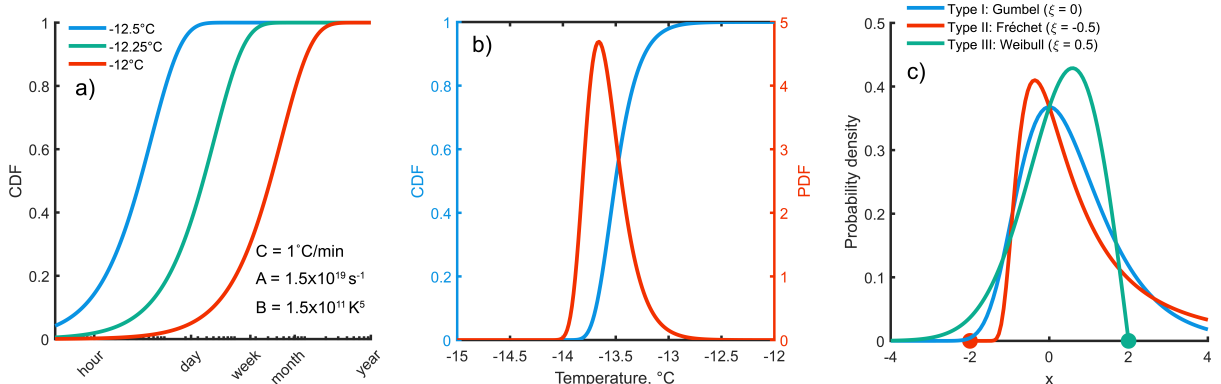


Fig. 9. Nucleation statistics a) Cumulative distribution function for isothermal supercooling (i.e., freezing probability). b) Survivor curve (blue/right) and probability density function for constant cooling rate. c) Extreme value distributions which describe distribution of heterogeneous nucleation active sites. Adapted with permission from Consiglio et al. [32].

In practice, these statistical relations provide the bridge between measured freezing temperatures and underlying nucleation physics, and they supply the most directly useful design quantities for cryopreservation. The statistical metrics summarized here underpin many of the emerging cryopreservation technologies discussed below. They enable rational selection of cooling and warming profiles, storage temperatures, and sample geometries that keep the cumulative nucleation probability acceptably low (for supercooling and vitrification) or, conversely, guarantee prompt nucleation at desired locations and times (for ice seeding and partial freezing). We will utilize these statistics in Case Study 2 later in this work.

2.3 Heat and mass transport

Now having formulated a description of the thermodynamic equilibrium states that cryobiological water may occupy and the molecular-level kinetic process that facilitates transition between these states, we arrive at the final physics that connect the practitioners and protocols of cryobiology to these phenomena—heat and mass transfer.

In practice, the cryobiologist has two principal means by which to control the outcome of a cryopreservation process, in terms of the final states attained and the phase transition route followed to arrive at those states: the first is chemical design of the cryobiological solution employed; the second is choice of thermal and mass transport history (cooling rates, warming rates, CPA loading rates, etc.). Historically, cryobiology literature has addressed the latter much more systematically than the former, and (for better or worse) much of the philosophy of cryopreservation protocol design today focuses on engineering of thermal and mass flow histories. Accordingly, there are many excellent reference works addressing cryobiological heat and mass transfer, and we will refer the reader to them rather than discussing comprehensively herein. We particularly recommend the formidable recent review by Zhao and colleagues [36], a salient chapter of the recent cryopreservation-focused *Annual Review of Heat Transfer* [37], and the Chapters of this book authored by Higgins and colleagues and Shu and colleagues.

Instead, we will here highlight the oft-overlooked intersections of heat and mass transport with the equilibrium thermodynamics and phase change kinetics at play, with a particular focus on relevant transport properties affecting those frameworks.

2.3.1 Heat transport - key concepts

The temperature history of a sample is one of the most important manipulable aspects of a cryopreservation protocol, underlying Mazur's famous two-factor hypothesis [21]; the process of vitrification [38]; and many other cryobiology essentials. However, the effect of this temperature history is nearly meaningless without its connection to the thermodynamics and kinetics at play, which it affects through the following broad aspects:

Temperature-time dependence of ice nucleation and growth

As described in the preceding section, the nucleation rate and probabilistic induction time of ice formation are functions of thermal history, a fact which may be leveraged in several ways. A few examples include: 1) During the slow freezing of cells, where extracellular ice nucleation is desired, the probable induction time of nucleation may be calculated as a function of cooling profile for the extracellular and intracellular compartments separately (even distinguishing only by compartmental volume), and a cooling profile that ensures a significantly smaller induction time for the extracellular compartment may be chosen. This is the principle behind “interrupted freezing” protocols [39]. 2) During the vitrification of any biologic, the cooling profile required to reach the glass transition temperature in less than one induction time (corresponding to perfect vitrification, and the most rigorous form of the “critical cooling rate”) may be estimated. 3) During supercooling, a cooling profile and storage temperature may be calculated such that the induction time for ice nucleation is much longer than the desired storage period. The cooling profiles required will be functions of both the underlying solution thermodynamics and the heterogeneous surfaces with which the system is in contact [32, 40].

Temperature-time dependence of metabolism & toxicity

The core mechanism enabling cryopreservation is the arrest of metabolism, which scales exponentially with temperature (see **Fig. 15** in Case Study 2 below). The toxicity of cryoprotectants, the rate of which

is driven both by the rate of metabolism and by the rate of various potential biochemical reactions and phase change processes, is likewise exponentially slowed upon cooling from normothermia. As a result, the temperature history of a given protocol is inextricably linked both to the plausible period of preservation achievable (based strictly on metabolism [41]) and to the toxicity accumulated by the sample. Thus, if the functional form of the temperature dependence of metabolism is known, metabolism arrest (i.e. preservation benefit) may thus be mathematically coupled to cryopreservation physics, as demonstrated by Consiglio et al. in the case of organ-scale supercooling [42]. Likewise, if the functional form of the temperature-dependence of toxicity rate is known, accumulated toxicity may be mathematically coupled to cryopreservation physics, as demonstrated by Benson and colleagues in the case of cellular vitrification [43–45].

Temperature-time dependence of thermomechanical stresses

Though a topic that has received comparatively minimal treatment historically, growing interest in cryopreservation of large biological samples (e.g. organs and organisms) has driven recent interest in the calculation and avoidance of thermal stresses that may accumulate due to either phase change or differential thermal contraction across a large, low-thermal-diffusivity sample during cooling. The first physics-based investigations of cryopreservation-related thermal stresses pertained to those developed during freezing [46], wherein the dynamic solidification front may drive significant local stresses. More recently, focus has turned to the considerable challenge of glass cracking during vitrification, which may manifest at even the microliter sample scale [47], and which proves especially challenging in the vitrification of macroscale tissues and organs [48, 49]. Cryopreservation thermomechanics presents a particularly rich intersection of solution thermodynamics and transport phenomena, with recent work demonstrating sharp dependences both on thermodynamic properties of the system (glass transition temperature, thermal expansion coefficient [50]), transport properties (thermal conductivity, viscosity), and precise sample geometry and localized temperature history [51].

Temperature-dependent thermophysical properties

We note finally that heat transport and the thermal history of a sample are coupled to every piece of physics described heretofore by the temperature-dependence of both thermodynamic properties (i.e. first or higher-order derivatives of the free energy, such as density, entropy, chemical potential, thermal expansion coefficient, heat capacity, etc.) and transport properties (thermal conductivity, viscosity, etc.). However, while this coupling is well appreciated, there remains an acute lack of low-temperature thermophysical property data for most solutions of interest to cryobiology (and a similar lack of predictive tools to cover this data gap), presenting a meaningful challenge to empirical accurate thermophysical description of various cryopreservation processes.

Gratefully, recent works indicate a growing, field-level effort to address this critical need for low-temperature and cryobiology-relevant thermophysical data. We point the reader to several key datasets commonly used in recent cryobiological modeling: that assembled by Rabin and colleagues, relevant to thermomechanics analysis of DMSO-based vitrification media [52, 53]; by Bischof and colleagues, relevant to critical cooling and warming rates for vitrification [54]; by Elliott and colleagues, relevant to melting point depression of various cryobiological solutions [10]; by Powell-Palm and colleagues, relevant to the viscosity of many-component aqueous solutions [55]; and by Consiglio and colleagues, relevant to high-pressure phase equilibria [19, 56, 57].

2.3.2 Mass transport - key concepts

Mass transport affects the practice and outcomes of cryobiology through various important processes and effects, both molecular (e.g. *via* the diffusivity of water in solution, which critically affects the nucleation process [58]) and biological (e.g. *via* the delivery of cryoprotectants across cell membranes [58]). Gratefully, a thorough treatment of cryobiological mass transport is provided in the Chapter of this book authored by Higgins and colleagues, covering delivery of cryoprotectants into cells, tissues, and organs (by both diffusion and perfusion), the fundamental role of osmotic stress in designing cryopreservation protocols, etc. For additional reading on the specific interplay between cryobiological mass transport and ice nucleation and growth processes, see these various references [58, 60–67].

3 Emerging techniques for cryopreservation of complex biomaterials

Armed now with sufficiently diverse thermodynamic theory to analyze the physical aspects of nigh-any cryopreservation protocol, we proceed to review emergent cryopreservation approaches through the lens of this theory. Our strategy in the text to follow is to provide an accessibly comprehensive survey of new or underexplored techniques and philosophies (and especially those for which alternative review works do not yet exist); to aid the reader in identifying and understanding the relevant physical theory guiding these approaches; and, where possible, to demonstrate the power of the theoretical tools articulated in **Section 2** to enhance both interpretation and practice of these protocols.

For consistency with our theoretical approach, we organize the emergent technologies discussed herein by the theoretical aspect—equilibrium thermodynamics, kinetics, or transport—that most principally drives their design or practice. We also include a final section dedicated to vitrification, as a prototypical technique drawing equally from all three aspects. For each section, we will review broadly the relevant techniques, then choose one on which to perform an illustrative case study in the application of relevant theory to meaningful, technique-specific analysis.

3.1 Equilibrium techniques

While all cryopreservation protocols are beholden to relevant phase equilibria (e.g. melting points, eutectic points) and thermodynamic properties (e.g. heat capacity, thermal expansion coefficient), only a particular subset are largely decoupled from the short time-scale phenomena associated with nucleation and transport processes. For these privileged few techniques, equilibrium solution thermodynamics dominate protocol design and practice, and they thus lend themselves to relatively simple (and powerful) first-order analyses.

3.1.1 Liquidus tracking

The technique perhaps most emblematic of the equilibrium-driven approach is *liquidus tracking*. As its name suggests, this approach aims to simultaneously introduce a cryoprotectant solution into a sample whilst reducing its temperature, such that the sample follows (in both composition and temperature) the liquidus curve of the solution (**Fig. 10**). By maintaining the sample at the lowest temperature at which the possibility of freezing may be systematically avoided (the liquidus temperature), this process minimizes cryoprotectant toxicity during loading to the highest degree achievable in a globally stable state, and provides the fastest means of cooling an organ to sub-0 °C temperatures (starting from a CPA-unloaded, supra-0 °C state) without accepting *any* degree of ice formation risk.

First proposed by Farrant in 1965 [68] and powerfully realized by Elford & Walter in 1972 [69], liquidus tracking in the modern era has been nigh-exclusively implemented as a CPA-loading strategy, as opposed to a final storage method. In practice, a sample is shuttled along an equilibrium concentration-temperature path towards a target final CPA composition, from which a final cooling step (typically to beneath the glass transition temperature) may then be performed with minimal risk of freezing (even while departing then from global equilibrium). This approach was formalized by Pegg and colleagues in the preservation of cartilage [70], wherein controlled stepwise introduction of DMSO and cooling of the sample, up to a terminal concentration of ~60% by mass and a terminal loading temperature of -70 °C (approximately 10 °C above the according liquidus temperature, as a margin of safety), permitted complete avoidance of ice formation during CPA equilibration, and achievement of tissue vitrification thereafter.

Pegg's approach, explored further in cartilage by his group [71], and in encapsulated 3D cell constructs by Fuller and colleagues [72], relied largely on preliminary empirical quantification of both liquidus temperatures as a function of composition, the rate or degree of CPA penetration at each step, and other protocol parameters. More recent work has advanced the technique towards its logical optimum, leveraging the imminent modelability of liquidus curves to predictively design optimal temperature-concentration protocols. In perhaps the most rigorous example of rationally-designed liquidus tracking to date, Shardt, Elliott and colleagues used solution theory (in particular multi-component osmotic-virial equations, as described in **Section 2.1**) to power calculate both liquidus coordinates and permeation driving forces for a multi-component CPA cocktail in articular cartilage, systematically reducing the time-toxicity profile of cryoprotectant loading to precede vitrification [59].

Finally, we note that while liquidus tracking has to date been applied only to diffusively loaded cell and tissue constructs, Wowk and Taylor et al. have proposed its use in perfusion-loaded vascular

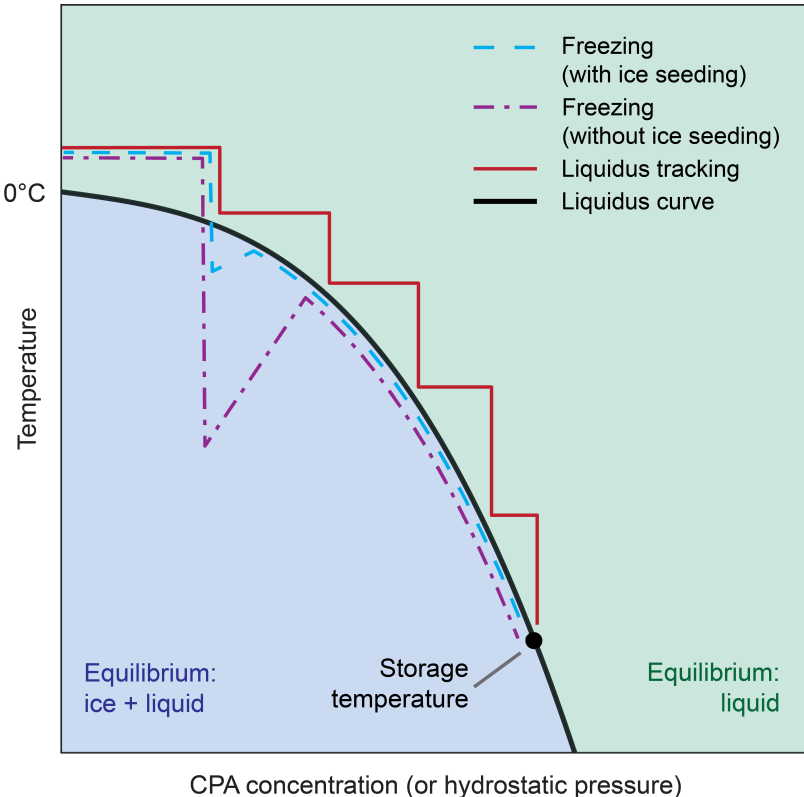


Fig. 10. Conceptual illustration of the thermodynamic paths followed by various equilibrium cryopreservation techniques. The liquidus curve, defining the melting point of ice as a function of CPA concentration or pressure, is given by the thick black line. In liquidus tracking (thin red line), a biological sample is simultaneously CPA-loaded and cooled, such that it follows the liquidus curve. This approach enables CPA-loading and sample storage at the lowest possible temperatures (and accordingly toxicities) at which the ice formation is not a risk. In partial freezing (dashed lines), a sample is loaded with an initial concentration of CPA, cooled below the liquidus, and allowed to form a two-phase liquid-ice solution. The amount of ice that will form at a given temperature is prescribed by the lever rule, and freeze-driven solute rejection will ripen the remaining liquid to the liquidus concentration at that same temperature. Seeding ice can minimize the osmotic shock accompanying this solute rejection (and mechanical damage from crystallization) upon initial nucleation from the supercooled liquid. Isochoric freezing follows an analogous thermodynamic path to partial freezing, but in either temperature-pressure space (if the liquid medium in the chamber is pure water, as is commonly used), or in 3D temperature-pressure-concentration space. We note that in partial freezing however ice forms *within* a biological sample, while in isochoric freezing ice forms *outside* of the sample.

systems, including whole organs [73, 74], and as a final storage technique independent of vitrification. In light of the following, we find this to be a promising route for future exploration: 1) recent studies in sub-0 °C whole-organ preservation have successfully utilized the *supercooled* liquid state for storage [3, 75–77]; 2) multi-pump, multi-thermic perfusion loading systems are increasingly becoming standard tools in organ cryopreservation; 3) metastable storage techniques using penetrating cryoprotectants only achieve ~1–2 °C supercooling, introducing freeze-risk that may outweigh the benefit of the marginally colder temperatures enabled; and 4) a wide diversity of new cryoprotectants show minimal toxicity at concentrations (3–6 molal [78, 79]) that may enable significantly colder preservation (~ –10 to –20 °C) than has yet been achieved in ice free preservation of whole organs.

3.1.2 Partial freezing

While liquidus tracking uses thermodynamic equilibrium to ensure complete avoidance of ice in a biological sample, the same liquidus equilibria may be leveraged to *allow* freezing in the sample but systematically limit its extent. This approach, demonstrated by Ishine, Rubinsky & Lee in the 1990s [80, 81] and later named “partial freezing” by Tessier, Toner, Uygun and colleagues [82–84], occupies the equilibrium corridor between liquidus tracking and classical slow-freezing, targeting temperature-composition coordinates that situate the sample beneath its liquidus temperature but above the eutectic temperature, rendering

a thermodynamically-stable two-phase liquid-ice equilibrium within, with the amount of ice prescribed by the lever rule (**Fig. 10**).

Use of partial freezing, as opposed to liquidus tracking, is motivated by the deeper temperatures of preservation achievable per-unit cryoprotectant loaded, at the cost of bulk ice formation. However, we note that *at equilibrium*, due to solute rejection, the cryoprotectant concentrations *in the portion of the system which remains liquid* will be precisely identical to those that would enable liquidus tracking at the same temperature, raising intriguing questions as to whether the benefits of reduced load concentrations outweigh the dangers of ice formation.

This technique has been developed principally for the preservation of vascular organs, in which a cryoprotectant solution may be delivered via machine perfusion or manual flush, and this ice formation may be strategically initiated in the vascular space, where it is hypothesized that it may nucleate, grow, and reject solutes with minimal mechanical interference. This initiation has been observed to accompany risk of damage to the endothelium [80, 82], both by mechanical mechanisms related to ice growth and biochemical mechanisms related to solute ripening. However, preliminary *ex vivo* evaluations of mammalian livers [82, 84] and kidneys [85] nonetheless appear promising.

In order to more deeply interrogate the thermodynamic and physical implications of partial freezing, and to demonstrate a prototypical thermodynamic analysis of a two-phase liquid-ice system, we conduct a Case Study of the partial freezing technique described by Tessier et al. at the end of this section.

3.1.3 Isochoric freezing

The vast majority of cryopreservation protocols are performed under a constant (typically atmospheric) pressure, wherein the volume of the sample may freely expand or contract in response to phase change, temperature change, composition change, or any combination thereof. In 2005, Rubinsky and colleagues proposed the opposite: to constrain the *volume* of a sample, thereby allowing its *pressure* to vary in response to these same changes [18]. This process, called isochoric (constant volume) or confined freezing, seeks to leverage hydrostatic pressure passively generated by the cooling process to depress the melting point of water, thereby protecting a biological sample from ice formation at temperatures beneath its atmospheric-pressure melting point.

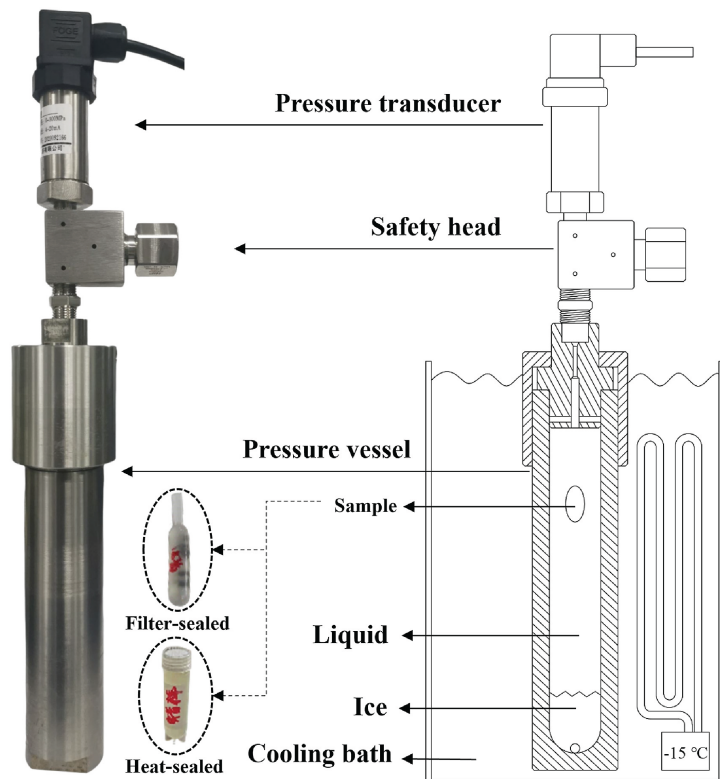


Fig. 11. Isochoric freezing chamber and schematic (adapted with permission from Lyu et al. [86]).

In practice, isochoric freezing typically involves submerging a biological sample in an aqueous medium within a rigid, high-strength chamber; sealing the chamber absent any air within; cooling the chamber to a sub-0 °C temperature; and initiating ice nucleation at a position in the chamber distant from the biologic (see **Fig. 11**). The growth and expansion of this ice will then, given its rigid confinement and isolation from the atmosphere, drive pressurization (on the order of 10–210 MPa) of the remaining liquid in the system (which contains the biologic), the melting point of which is in turn depressed until the ice and liquid achieve a two-phase equilibrium, as prescribed by the pressure-temperature-composition (p-T-x) liquidus curve.

As such, isochoric freezing represents the same thermodynamic principle as partial freezing: ice is deliberately nucleated and allowed to “ripen” the remaining liquid (whether in concentration, in pressure, or in both) until thermodynamic equilibrium is reached. However, two key differences distinguish these techniques. First, in isochoric freezing, the limited formation of ice within the system occurs *outside* the biological sample, as opposed to within it, thereby providing ice-free preservation at sub-0 °C temperatures. Second, isochoric freezing may be practiced with or without cryoprotectants, as pressure depresses the melting point of liquid water universally. As such, cryoprotectants in isochoric freezing carry only a portion of the burden of ice protection, enabling ice-free preservation at lower cryoprotectant concentrations at a given temperature [87, 88]. However, just as the temperature advantages of partial freezing are weighed against the potential dangers of ice formation, so the advantages of isochoric freezing are weighed against the potential dangers of pressure.

For a deeper discussion of the principles of isochoric freezing, in addition to a comprehensive summary of its application to multi-scale biologics ranging from mammalian hearts to fresh food products, we refer the reader to our recent review of this topic [19].

3.1.4 Case study 1: Thermodynamic analysis of chemical evolution during partial freezing

Partial freezing, in the limit of prompt nucleation and slow cooling rates, lends itself to straightforward analysis with the toolkit of equilibrium solution thermodynamics. In this Case Study, we will demonstrate simple applications of this toolkit to the interrogation of a partial freezing solution and protocol reported by Tessier et al. [1], and in doing so illustrate routes towards rational design of partial freezing solutions and protocols. A general process is as follows:

1. Select a multi-solute solution thermodynamics model to describe the chemical potential of the partial freezing solution of interest and utilize it to calculate the melting point.
2. Acknowledging that ice forms a pure solid phase, effectively removing water the liquid solution, calculate the partial freezing-relevant liquidus curve by iteratively decrementing the concentration of water whilst holding all other component concentrations constant, and re-calculating the melting point for each decrement.
3. Use this liquidus curve and the lever rule to calculate the amount of ice that will form at a given sub-freezing temperature, as a fraction of the total system mass or volume. Calculate the according concentrations of total or individual solutes by removing the calculated amount of ice from the initial liquid water content of the solution and re-calculating the concentrations.
4. Use these insights to choose an appropriate storage temperature, based on desired limits of ice formation, terminal concentrations of cryoprotectants or electrolytes in the unfrozen liquid phase, etc. Alternatively, use the steps above to *design* a solution that provides optimal values of the aforementioned.

Using the partial freezing solution composition provided by Tessier et al., we show prototypical outputs of this process in **Fig. 12**. For each of the three variants investigated by the authors (which differ only in the choice of penetrating cryoprotectant, held at 12% vol/vol) we use the multi-solute osmotic virial equation to calculate the chemical potential of the liquid, and its relation to calculate the melting point (see **Section 2.1**). Solution recipe and all virial coefficients are shown in **Table 1** (note that we approximate the 3-O-methyl-glucose employed as glucose monohydrate, as thermophysical properties of the former are not available). Electrolytes for which virial coefficients are not available are treated as ideal. We calculated the unfrozen solution osmolalities and melting points to be $\pi_0 = 3.16$ Osmol/kg and -5.9 °C for propylene glycol, be $\pi_0 = 3.07$ Osmol/kg and -5.7 °C for glycerol, and $\pi_0 = 3.8$ Osmol/kg and -7.1 °C for ethylene glycol.

In **Fig. 12**, for each choice of penetrating cryoprotectant, we show the fraction of the system that freezes, the total solute concentration in the remaining unfrozen liquid, and the individual concentrations of each component as functions of temperature at thermodynamic equilibrium. Several salient insights

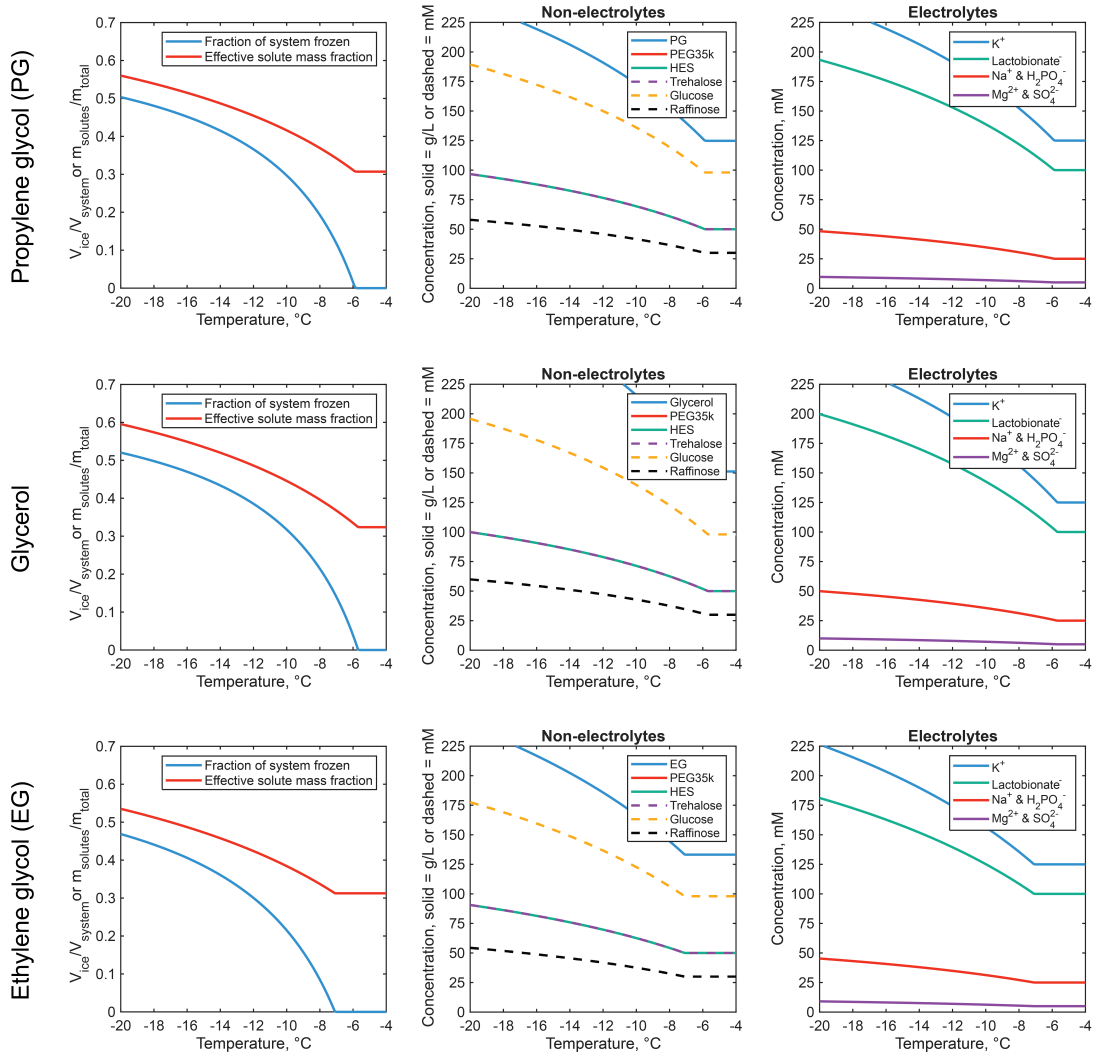


Fig. 12. Thermodynamic analysis of a partial freezing solution. We analyze the compositions reported by Tessier et al. [1], which vary only by the choice of penetrating cryoprotectant. Results for each cryoprotectant are organized by row as labeled. The first column gives the ice fraction and the effective solute mass fraction in the remaining liquid phase at thermodynamic equilibrium, as a function of temperature. The second and third columns give the freeze-driven evolution of the concentrations of each chemical component as a function of temperature.

emerge, which we may evaluate against the observations of Tessier et al. in their histological and functional evaluations of partially frozen rodent livers.

They first investigated differences between the three cryoprotectants at -10°C , observing glycerol to be broadly damaging across metrics, and the two glycols to be less so (though in different respects). Regardless of the known osmotic drawbacks of glycerol attributable to its slow penetration, these findings appear generally predictable based on **Fig. 12**, which shows that glycerol both allows the most ice formation and drives the largest electrolyte imbalances in the remaining liquid phase (e.g. $\sim 178\text{ mM}$ potassium) at -10°C . Amongst ethylene glycol and propylene glycol, the authors observed marginally superior structural preservation (in histology) for ethylene glycol, consistent with its relatively lower ice fraction, but marginally worse functional outcomes in some cases nonetheless, which may be attributable to mild differences in biochemical toxicity or osmotic stress profile of the CPA at sub-0 $^{\circ}\text{C}$ temperatures, or an insufficient normothermic perfusion timeline to observe complete recovery, which has been found in select other models to take longer than one hour after prolonged sub-0 $^{\circ}\text{C}$ storage [91].

The authors proceeded to investigate propylene glycol at -10°C and -15°C , finding that storage at -15°C , despite the putative benefit in metabolism reduction (see **Fig. 15d** in Case Study 2), yielded more extensive hepatocellular injury, loss of liver sinusoidal endothelial cells, and ultimately poorer functional outcomes. Per **Fig. 12a**, this additional morphological and endothelial damage is likely a consequence

Table 1. Partial freezing solution and corresponding osmotic virial parameters. Solution composition from Tessier et al. [1] and virial parameters from Zelinski et al. [89] (PEG-35,000 virial coefficient from Wang et al. [90]).

Component	k_{diss}	B_i	C_i	g/L	mM	mol/kg
HES	1	35.29	-1.107×10^7	50.00	0.25	3.38×10^{-4}
Lactobionic Acid	1	0	0	35.83	100	0.135
Potassium Phosphate monobasic	2	0	0	3.40	25	0.0338
Magnesium Sulfate (heptahydrate)	2	0	0	1.23	5	0.00674
Raffinose (pentahydrate)	1	0.08	0	17.83	30	0.0405
Potassium Hydroxide	1	0	0	5.61	100	0.135
Sodium Hydroxide, 5N	1	0	0	1.00	25	0.0338
PEG-35,000	1	5200	0	50.00	1.4	0.00193
Trehalose (dihydrate)	1	0.12	0	18.92	50	0.0676
Glucose (monohydrate)	1	0.044	0	19.42	98	0.132
Propylene glycol	1	0.039	0	124.8	1640	2.22

of the nearly 50% increase in ice fraction (from ~ 0.3 to ~ 0.44) upon shifting from -10 °C to -15 °C. Intriguingly, the total intercellular space in the liver has been measured as ~ 30 -40% of the total liver volume [92], which may further explain the relative palatability of partial freezing at -10 °C, though it is unclear whether functional degradation is driven more by mechanical aspects of ice formation, or by the rate and degree of electrolyte ripening in the remaining liquid phase (which is of course coupled to said ice). We note that in later work [84], the same authors saw somewhat improved outcomes at -15 °C upon incorporating more polyethylene glycol, which may serve to retard both ice growth and the diffusion of rejected electrolytes, thereby reducing the sharpness of mechanical or osmotic shock experienced.

These simple analyses both help to interpret past experimental outcomes and suggest design approaches to for future partial freezing protocols. For example, by altering the electrolyte concentrations in the starting media, a solution could easily be designed which achieves the desired sodium/potassium balance *only at sub-0* °C equilibrium, rather than allowing the significant excursions seen here. Specific ice growth limits may also be easily targeted; different candidate cryoprotectants may easily be screened; and etc.

3.2 Kinetic techniques

The techniques described in the preceding section are unified by their concern with achieving or maintaining stable thermodynamic equilibrium, wherefrom additional spontaneous evolution of the system (e.g. phase change, compositional change) becomes impossible. As such, from a thermophysical perspective, these techniques are driven by phenomena with long-to-infinite associated time scales, and depend only minimally on acutely transient processes. However, many cryopreservation protocols may deviate significantly from this equilibrium, passing through (or deliberately occupying) a metastable supercooled state wherefrom ice nucleation, whether desirable or to be avoided, is strongly *time* dependent, and for which temporal aspects of the protocol are key. In this sub-section, we will review several emerging techniques dominated by kinetic aspects of ice nucleation and growth, seeking to interpret each within the kinetic framework described in **Section 2.2**.

3.2.1 Ice seeding

Kinetic techniques in general seek either to *accelerate* or *delay* the nucleation of ice upon cooling beneath the melting point. The process of *accelerating* nucleation is often referred to as “ice seeding”, and is typically desired for two reasons: 1) to avoid the excessive mechanical, thermal, and osmotic damage that can occur if extracellular nucleation occurs at deeply supercooled temperatures, and 2) to avoid intracellular ice nucleation entirely, by enabling extracellular ice growth and solute rejection to gradually draw water out of (and force cryoprotectants into) the cell, thereby stabilizing it against nucleation as it reaches ever-colder temperatures.

As such, within the formalism of nucleation theory, ice seeding protocols must be designed such that the induction time of ice nucleation in the extracellular space is much shorter than that in the intracellular space. While the relative volume of a given cell compared to the extracellular space already favorably biases these induction times, this bias is typically insufficient to avoid the mechano-osmotic damage that can be associated with rapid extracellular ice growth. As such, emergent approaches to ice

seeding focus on means to further shift the induction time of extracellular nucleation forward, using both passive approaches (e.g. ice nucleating agents (INAs)) or active approaches (e.g. ultrasonication). Many excellent works over the past decade have reviewed both the fundamentals of and progress in ice seeding [93–95]; as such we will here review only the most recent advances in the field.

Passive methods of ice seeding focus on increasingly effective ice nucleating agents, which leverage heterogeneous nucleation modes to induct ice formation at temperatures ever-closer to the equilibrium melting point of the solution. Historically, the *SnoMax* ice nucleating bacteria, silver iodide, and a small clutch of other nucleators were used to this end, but the past half decade has seen a rapid expansion in INA offerings. Key materials of recent interest include: 1) several varieties of naturally-occurring mineral, including various feldspars, quartz, and the “hyperactive” K-feldspar LDH1, which has been found to enable nucleation at <1 °C supercooling [96]; 2) emergent classes of nature-derived water soluble organic materials, including polysaccharides from the pollen *Carpinus betulus* (or European hornbeam) [97], hydrated cholesterol [98], etc.; and 3) ice nucleating bacteria, including previously unrecognized members of the Pseudomonadaceae, Enterobacteriaceae, Xanthomonadaceae and Bacillaceae families [99]. These molecules nucleate ice through a wide host of divergent hypothesized mechanisms, from crystalline templating / interfacial free energy reduction to specific bacterial protein interactions, significant headroom remains in our understanding of passive ice nucleation processes.

Active methods meanwhile do not involve additives to solution. One popular such method in recent years is nucleation by acoustic or ultrasonic stimulation, which is generally understood to drive cavitation effects that yield massive hyper-local fluctuations in pressure that produce ephemeral nuclei of high-pressure ice phases, which then seed hexagonal ice [100]. Ultrasonic ice seeding has shown beneficial results in the preservation of samples ranging from hepatocytes to fresh food products [101–103], though significant additional work is needed to develop a physics-first understanding of optimal sonication parameters for nucleation. As evidence, it should be noted that ultrasound is also drawing considerable recent attention as a means of supplying rapid warming for large biological samples, wherein the goal is to *avoid* ice formation *en route* from the vitrified state [103].

3.2.2 Supercooling

As we have established throughout this chapter, the induction of ice nucleation upon cooling beneath a solution’s melting point occurs over a finite and probabilistically quantifiable time scale. If this time scale is greater than the desired preservation time for a given experiment, the solution may remain at metastable equilibrium in a supercooled liquid state, thereby enabling ice-free preservation at sub-0 °C, sub-melting point temperatures.

Supercooling, though recently reaching new heights of popularity as means of practical stabilization have expanded, is one of the foundational concepts of cryopreservation for complex biological systems, seen both in the literature for >60 years and in nature for millennia. Supercooling as a fundamental mode of *self*-preservation in nature has been corroborated time and again across organismal complexities, from single-celled fungi (e.g. yeast, demonstrated by Franks and colleagues to stably supercool at -20 °C for >16 weeks [104]) to whole mammals (e.g. the arctic ground squirrel, demonstrated to supercool at ~ -3 °C for months of winter on end [105]), and has inspired the recent advent of supercooled cell [106], tissue [107], and organ preservation [3, 75–77, 108, 109].

From a physical perspective, the principal challenge of supercooling is ensuring the *stability* of the supercooled state, or the probability that nucleation will occur (i.e. the induction time will be reached) within the desired preservation period. In the modern era, select intersecting approaches to supercooling stabilization have emerged in biopreservation contexts, though many more may be imagined based on the principles described in this chapter.

Usta and colleagues discovered that the liquid-air interface contributes in a uniquely potent fashion to heterogeneous ice nucleation in supercooled solutions, and that this contribution may be reduced in large part by sealing the exposed surface of the solution with an immiscible layer of liquid (e.g. mineral oil). This principle has since been deployed extensively in the supercooling of various sensitive cell models [106, 110–114], and to a lesser degree in preservation of mammalian livers [3, 75] and kidneys [115] (wherein chemical stabilization is the dominant driver; see below).

Powell-Palm and colleagues then identified that isochoric or confined conditions (embodied by sealing the system of interest in a rigid, air-free container) further stabilized the supercooled state [40], driven by a suite of non-chemical mechanisms including the air-avoidance identified by Usta [116], isolation against vibration [117, 118] and density fluctuations (which are necessarily unconstrained in open systems with access to atmospheric pressure), and putative atomistic effects on the nucleation barrier [119]. A

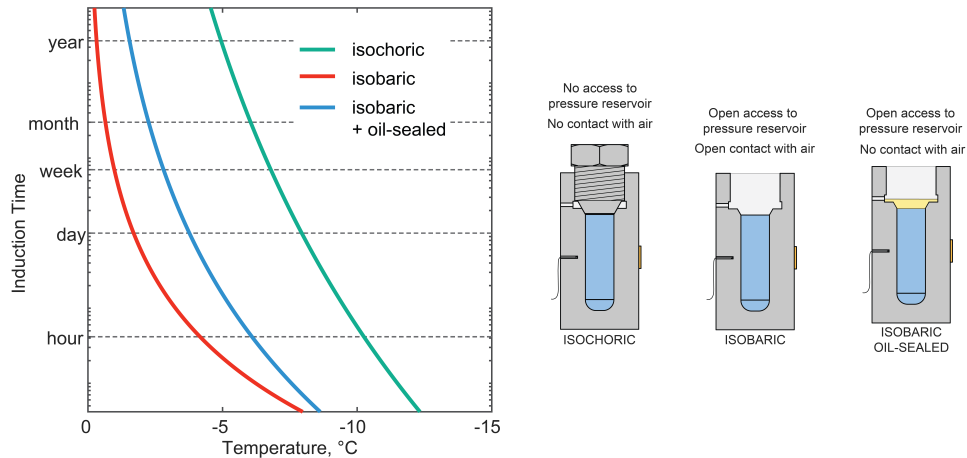


Fig. 13. Nucleation induction times as a function of temperature for isochoric (green), isobaric (red), and oil surface sealed isobaric (blue) systems (left) and corresponding schematics of systems (right). Adapted with permission from Consiglio et al. [40].

comparison of nucleation induction times in pure water for both these techniques (and an open, unaffected sample) are shown in **Fig. 13** (adapted from Consiglio et al. [40]). Isochoric supercooling has since been deployed in the preservation of cells, engineered tissue constructs, mammalian livers, and mammalian hearts, in addition to a variety of fresh food products [19].

It is critical to note that the two mechanisms above, oil sealing and isochoric supercooling, present *purely physical, non-chemical* means of stabilizing the supercooled state—i.e. they do not require that any particular chemical composition be introduced into the supercooled biologic. However, while this non-chemical nature is no doubt favorable from a regulatory perspective (and enables interrogation of purely temperature-dependent biopreservation phenomena, absent ice and absent chemical confounders), nothing *precludes* these techniques from being *coupled* with chemical interventions to further stabilize supercooling, as noted previously by Taylor et al. [74].

An initial demonstration of this combination was provided by the group of Toner and Uygun, who coupled oil-sealing with penetrating cryoprotectants and high-molecular weight polymers to achieve multiday supercooled preservation of the human liver, providing a watershed moment in the demonstration of the applicability of the technique to transplant medicine. However, despite this blend of stabilizing effects, supercooling was only achieved to ~ 1 °C beneath the melting point (-4 °C storage temperature) [3]. More recently, Huang and colleagues have realized this premise to a much greater degree, obtaining supercooling to ~ 9 °C beneath the melting point (-10 °C storage) in rodent kidneys [115]. To achieve this, they combined oil-sealing with a preservation solution that includes the synthetic ice blocker 1,4-cyclohexanediol alongside multiple polymers, each at molecular weights at which they will both leave the vascular space (i.e. enter the interstitium) and plausibly provide molarity-disproportionate depression of the nucleation temperature [120, 121]. Huang and colleagues note, as we have also previously [19], that even deeper supercooling may likely be achievable by combining this chemical approach with isochoric supercooling. A survey of recent organ supercooling studies is shown in **Fig. 14**.

The practical utility of supercooling, especially for large, ultra-high-value biologics like transplantable human organs, is a strict function of the likelihood of ice formation at the desired storage temperature, in the precise configuration to be used. While for many years the probabilistic nature of ice nucleation had been considered an insurmountable difficulty in achievement of a reliable technique, recent work (borrowing from long-standing insights in metallurgy and phase-change thermal energy storage) has leveraged the robust mathematical describability of memoryless activated stochastic processes to powerfully constrain the nucleation probability space, enabling rational design of *safe, stable* supercooling protocols by leveraging the very stochasticity that previously appeared a liability. Using constant-cooling-rate or isothermal nucleation experiments, the theory described in **Section 2.2.5** of this chapter may be used to calculate an induction time isopleth for a given probability of ice nucleation (say, 1-in-10,000), thereby enabling quantification, from an empirical, protocol- and system-specific basis, of a safe supercooling duration. In Case Study 2, we detail this thermodynamic-kinetic approach to “supercooling engineering”.

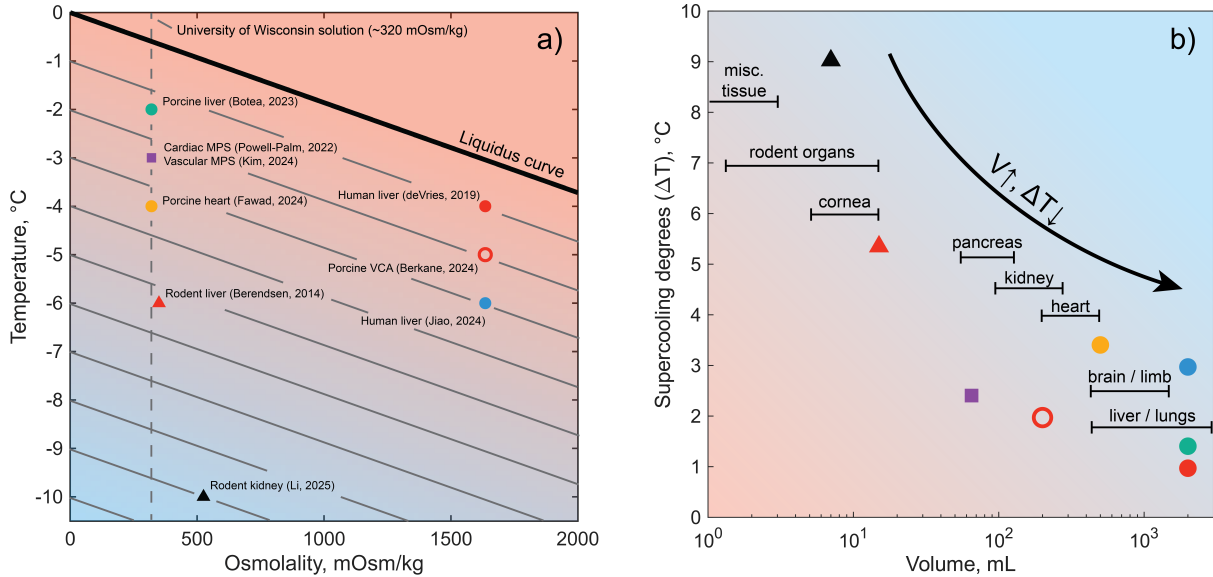


Fig. 14. Recent progress in supercooling for organ preservation. a) Supercooling temperatures reported for organ and organoid models as a function of the osmolality of the solution used [3, 75–77, 91, 107–109, 115]. Thin gray lines represent supercooling isotherms, along which the distance in temperature from the melting point is constant. b) Degrees of supercooling past the melting point (i.e., ΔT) for the same solutions as a function of sample volume. The volume ranges corresponding to various human organs and tissues of interest in transplantation are indicated by horizontal black bars. The exponentially inverse correlation between sample volume and supercoolability is consistent with classical nucleation theory and the extreme value interpretation of nucleation statistics [32, 122, 123].

3.2.3 Case study 2: Rational engineering design of supercooling protocols

Using the statistical nucleation kinetics framework described in **Section 2.2.5**, benchtop nucleation experiments may be used to rigorously design supercooling protocols with arbitrarily high margins of safety against nucleation, or arbitrarily low probabilities of ice nucleation at a desired temperature or a desired storage period. The general process is as follows:

1. For the specific container type, sample volume, and sample composition of interest, perform multiple constant cooling rate nucleation temperature tests in order to assemble a distribution of nucleation temperatures (a “survivor curve” or cumulative distribution). A minimum of ~30 replicates is recommended to robustly capture intra-sample variance (i.e., using *precisely* the same sample repeatedly), a process that can be informed by computing confidence intervals (e.g., through bootstrapping).

a) *Note: If these replication numbers prove untenable at full sample volume due to cooling rate or other limitations, scaled-down versions of the desired system may be used, and surface area or volume-based scaling rules may be applied to adjust the results as needed [32].*

2. Fit a non-homogeneous Poisson distribution (Equation 47) to this data in order to extract the temperature-dependent system nucleation rate [40]. Use this rate to calculate the probability of ice nucleation at desired storage time or/and the induction time for a desired probability of nucleation as functions of temperature.

3. Repeat steps 1 and 2 with different samples in order to capture inter-sample variance. Take worst case trial (most nucleation prone), average trial, or apply extreme value statistical methods in order to compute the overall freezing probability [32].

4. Identify a combination of storage temperature and storage time that provide the desired margin of safety on supercooling stability (e.g., a 1-in-10,000 chance of ice nucleation). For any given physical system/container with the same heterogeneous nucleation characteristics (i.e. same surfaces in contact with the liquid, same closure conditions, etc.) as captured in the underlying nucleation data from Step 1, extrapolate these results in sample volume, surface area, or solution composition using available physical and thermodynamic scaling rules to further explore the opportunity space.

Using data from Consiglio et al., we show sample outputs of this process in **Fig. 15** (for a single sample). We use the preferred form $J = A \exp\left(-\frac{B' T_m^5}{T^3 \Delta T^2}\right)$ to capture the temperature dependence of the nucleation rate, with parameters $A = 2.01$, $B' = 1.07$, representing data for 1 L pure water contained

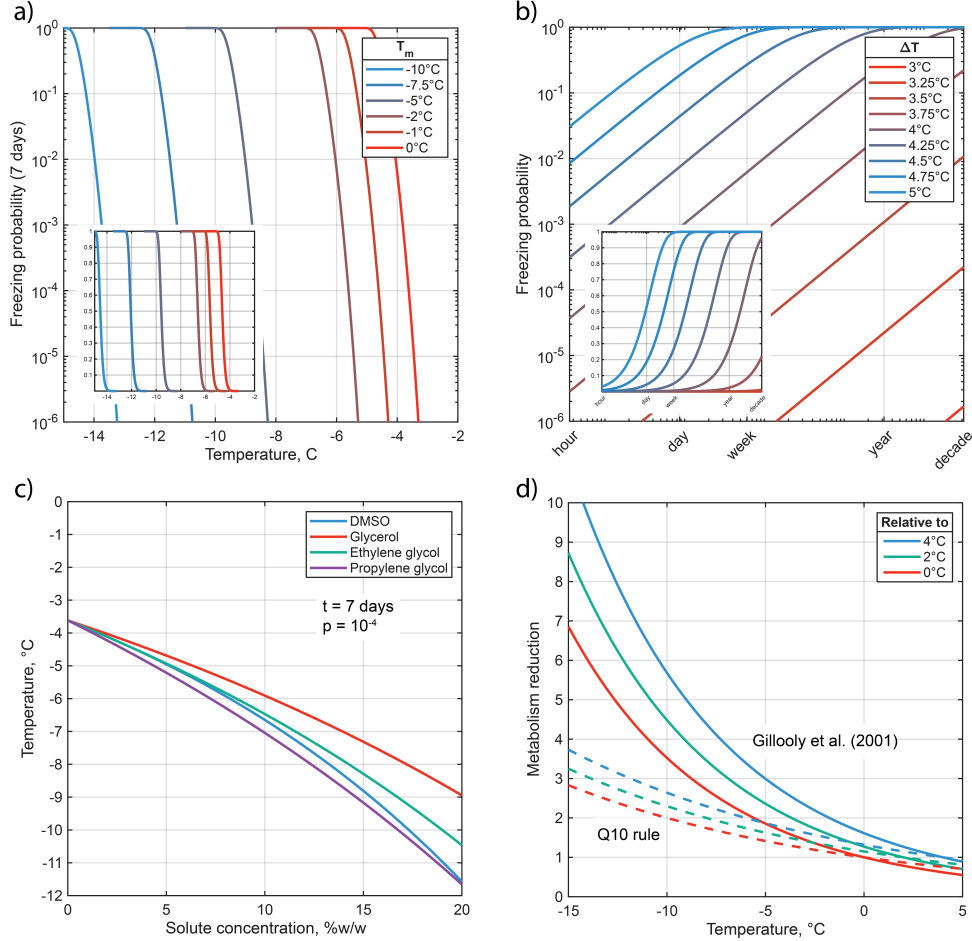


Fig. 15. Kinetics insights for the rational design of safe supercooling protocols. Panels and methodology described in detail in the text above. a) Freezing probability for 7 days of supercooling at a given temperature, for solutions of varying melting temperatures. b) Temperature to which a solution may be supercooled for 7 days with a 1-in-1000 chance of freezing, for aqueous binary solutions of four common cryoprotectants. c) Freezing probability versus time for varying degrees of supercooling past the melting point. d) Factor of metabolism reduction relative to various conventional cold storage temperatures as a function of supercooling temperature. Dashed lines represent the oft-cited (though woefully poorly supported) notion that metabolism is reduced by half for every 10°C of cooling. Solid lines represent the landmark empirical metabolism model of Gillooly et al. [41].

within an isochoric container, and in direct contact only with a uniform petrolatum coating on the chamber walls (see Fig. 5 of Consiglio et al. [32]). The freezing probability is calculated as $p = 1 - e^{-Jt}$.

In **Fig. 15a**, we show the probability of freezing in a 7-day period as a function of solution melting point. Here, the $T_m = 0^\circ\text{C}$ curve is calculated according to the steps above from the benchtop data described, and the $T_m < 0^\circ\text{C}$ data utilize the assumption that, in the dilute limit, the nucleation parameters A and B are insensitive to the concentration of conventional permeating CPAs. This assumption reproduces the common observation that the ratio λ of nucleation temperature depression to melting temperature depression is equal to 1 for solutions at bulk volumes dominated by heterogeneous nucleation [40, 124]. We note however that $\lambda \sim 2$ in the same solutions when in emulsified or atmospheric droplet forms susceptible to homogeneous nucleation. Furthermore, solutions with polymeric additives may reach $\lambda \gg 2$ (whether heterogeneously or homogeneously nucleating), a phenomenon which Powell-Palm et al. have attributed to the dominant role of the configurational entropy of the liquid in prescribing the liquid-ice interfacial free energy [9].

Using the same data, in **Fig. 15b**, we show the probability of freezing as a function of degree of supercooling $\Delta T = T_{\text{melting}} - T_{\text{supercooling}}$. In **Fig. 15c** we show the temperatures to which four common binary water-cryoprotectant solutions are predicted to stably supercool for 1 week with a 1-in-1,000 chance of ice nucleation. Equilibrium melting temperature curves are calculated via the osmotic virial equation (see **Section 2.1**).

Finally, in **Fig. 15d**, we show an additional essential consideration in choosing a desired supercooling temperature - the degree of metabolic suppression putatively achieved at that temperature. Here, dashed lines show the factor by which metabolism is suppressed relative to ≥ 0 °C classical storage temperatures according to the oft-cited “Q10 rule”, which supposes that the rate of metabolism halves for every 10 °C of cooling from normothermia. This “rule” is based simply on the requirement of Arrhenius scaling for the biochemical reactions of which metabolism is comprised, and not life-specific theoretical or empirical data. As a data-driven alternative, we also provide the reduction in metabolism predicted for mammals by the landmark empirical model of Gillooly et al. [41]. While their model is based on data between 0 °C and 37 °C, we argue that this scaling provides much better agreement with the last decade of preservation extension observed in studies on supercooling of complex biological systems.

In total, **Fig. 15** conveys the rich variety of physicochemical information that may be used to rationally design safe and reliable supercooling protocols, requiring only straightforward benchtop nucleation temperature experiments and elementary statistical kinetics calculations.

3.2.4 High pressure freezing

High-pressure freezing (HPF) exploits the strong pressure-dependence of water’s phase diagram to kinetically suppress ice formation during cooling, enabling vitrification or near-vitrification with substantially lower cryoprotectant concentrations than are required at atmospheric pressure. Raising pressure shifts the liquid–ice coexistence line and reduces the driving force for nucleation and growth at a given temperature.

In conventional HPF devices adapted from electron microscopy, small specimens (typically ≤ 200 μm thick) are rapidly pressurized to ~ 200 MPa and simultaneously cooled by a high-velocity liquid nitrogen jet or similar. Recent work shows that such platforms can be repurposed from cryo-fixation to cryopreservation [125], with 2D monolayers and 3D spheroids vitrified at ~ 210 MPa with only 20–30% v/v permeating CPA plus non-penetrating polymers displaying higher post-thaw viability, metabolic activity, and retention of cell-cell junctions than comparable normal-pressure plunge-freezing protocols.

Closely related “self-pressurized rapid freezing” (SPRF) approaches achieve comparable pressures without an external pressurization system by rapidly cooling sealed capillaries or microchannels [126, 127] completely filled with aqueous media, absent air. Initial ice expansion in the confined volume raises internal pressure into the 10s to 100s MPa range, and the system follows an effectively isochoric path in which further ice growth is disfavored. HPF and SPRF thus sit at the intersection of equilibrium and kinetic considerations, where pressure first reshapes the liquidus surface, then consequently weakens the thermodynamic driving force for ice formation.

3.3 Transport-driven techniques

As we have argued thus far, cryopreservation, as a process dependent on the management of phase change, is driven principally by equilibrium thermodynamics and nucleation and growth. While these phenomena obviously intersect with and are dependent upon heat and mass transport in many critical ways, techniques truly *driven* by transport phenomena (i.e., moreso dependent on transport than on the underlying thermodynamics and kinetics at play) are comparatively rare. In this sub-section, we will review two such techniques.

3.3.1 Directional freezing

Directional freezing consists of advancing a biologic across a known (typically linear) temperature gradient in order to control the speed and position of the freeze front and ensure uniformity of freezing conditions. Introduced first by Rubinsky & Ikeda [128] as an analytical tool with which to investigate ice front geometry and cell–ice interactions, the technique has since been applied as a means of minimizing damage associated with ice growth during preservation of biological samples across scales.

Directional freezing devices typically utilize two constant-temperature heat sinks, one at a temperature above the melting point of the biological sample of interest and the other below, separated by a gap of known length. A conducting substrate of low thermal mass is then placed across sinks, such that the portion spanning the gap assumes a constant, approximately linear temperature gradient between the two. A biological sample in solution is then placed in intimate thermal contact with this plate, nominally fixing its temperature to its position in the direction of the gradient, and producing a freeze front perpendicular to this direction at the position corresponding to the melting point. The sample is then

slowly advanced from the warm side to the cold, such that its cooling rate is a function only of its linear velocity (see schematic in **Fig. 16**).

By then controlling this sample velocity, directional freezing fixes the local cooling rate at the moving freeze front, converting what is ordinarily a spatially and kinetic heterogeneous freezing process into a high-deterministic moving-boundary problem, describable by the classical Stefan formulation [129]. Furthermore, given that latent heat and rejected solutes may both be evacuated in a prescribed direction (into the unfrozen portion), multi-site nucleation and re-melting related to recrystallization events are suppressed, and solute concentration gradients remain approximately constant at the freeze front during freezing. In principle, directional freezing thus enables freezing of an entire biological sample at a uniform cooling rate, solute-rejection rate, etc.

In practice, this approach has been productively utilized in a variety of samples for which the optimal aspect ratio for enforcement of the linear temperature gradient by conduction (footprint dimensions \gg thickness) can be obtained. For adherent cellular monolayers, Braslavsky and colleagues [130] have shown that a two-step implementation incorporating an initial directional freeze to $-20\text{ }^{\circ}\text{C}$ followed by conventional slow cooling to cryogenic temperatures has been shown to markedly improve post-thaw attachment and viability relative to conventional slow cooling alone. Others have shown similar benefit in the freezing of spermatozoa across multiple species and multiple cell suspensions [131–134], where uniform front propagation mitigates localized crystallization and solute pocketing that otherwise accompany uncontrolled freezing.

Directional freezing has also been investigated to a very limited degree at tissue and organ length scales, for which increasingly sophisticated stages involving multiple temperature gradients have been developed [135]. Notably, Arav and co-workers have demonstrated improvement in frozen preservation of both ovarian tissue slices [136–138] and whole sheep ovaries, some of which proceeded to produce hormonal activity upon thawing and transplantation. However, significant additional research effort is needed to establish potential utility of the technique for organ-scale biologics, and scaling analysis by Ukpai & Rubinsky suggests that samples above $\sim 1\text{ cm}$ characteristic thickness cannot be directionally frozen in a uniform fashion with the standard single-conductive-substrate configuration [129].

We also note that directional freezing presents a purely physical tool for modulation of freezing behaviors, and thus may be coupled with related chemical techniques, producing for example “directional partial freezing” or “directional isochoric freezing”.

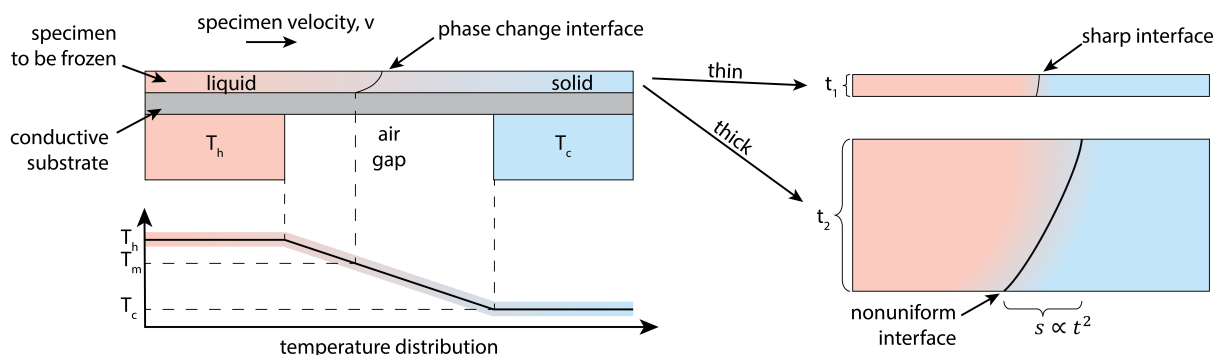


Fig. 16. Illustration of a typical directional freezing platform. A biological sample is advanced along a conductive substrate with an imposed (typically linear) temperature gradient, such that its velocity controls the rate at which the liquid-ice phase change interface moves through the sample (i.e. the freezing rate). As demonstrated by Ukpai & Rubinsky [129], while this interface is often assumed “flat”, or perpendicular to the direction of the temperature gradient, it is only so for extremely thin samples, and scaling analysis suggests that uniform directional freezing of biologics with greater than $\sim 1\text{ cm}$ thickness cannot be achieved using conventional single-plate conduction in a room temperature atmosphere.

3.3.2 Spray, droplet, and flash freezing

Since Birdseye’s foundational discovery in the 1920s that faster cooling produces smaller ice crystals, rapid-cooling approaches have become integral to both microscale preservation of cellular products and macroscale preservation of fresh food products [139–142]. In industrial contexts, a broad class of high-heat-flux freezing technologies—including cryogenic freezers, impingement freezers [143], fluidized bed

freezers, and immersion freezers [144]—leverage large convective coefficients (up to ~ 2000 W/m²), thin thermal boundary layers, and varied sub-0 °C refrigerants (e.g., liquid or high-velocity gaseous nitrogen, air at -40 °C, ethanol mixtures, etc.) to achieve high cooling rates in mL- to L-scale food products, thereby maintaining post-thaw quality by reducing characteristic crystal size, drip loss, and textural degradation [140]. Intriguingly, while such macroscale rapid cooling platforms are omnipresent in the food preservation domain, they have not yet been widely applied to rate-dependent whole organ or large organism cryopreservation efforts (see vitrification section below), suggesting potentially low-hanging opportunities for translational engineering efforts in the near future. As noted in the excellent review by James et al. [144], this may be a consequence in part of knowledge in state-of-the-art food rapid freezing technologies being disseminated through industrial pathways, rather than through conventional scientific publishing.

At smaller scales, droplet- and spray-based rapid freezing methods pursue the same transport objective by reducing the characteristic thermal length scale. Cell-laden pL- to uL-scale droplets produced by atomizing nozzles, microfluidic droplet generators, or inkjet heads, when deposited on cryogenic substrates or into cryogenic liquids, can achieve cooling rates in excess of 10^4 – 10^6 °C/min, sufficient to restrict crystalline ice growth to within tolerable limits even with little-to-no penetrating cryoprotectants [145–148]. For a more in-depth discussion of droplet-scale cryopreservation approaches, see the Chapter of this book authored by Zhao and colleagues.

3.4 Vitrification

At long last, we reach that technique which above all others defies clean placement in one or the other of the preceding categories: vitrification. First explored for cryopreservation purposes by Luyet & Hodapp in 1938 [149], vitrification describes the process of shuttling an ice-free biological sample into and out of the glassy state, and represents the most thermophysically complex cryopreservation process yet devised. Successful practice of this technique requires an extremely delicate balance between thermodynamic, kinetic, and transport considerations, all of which grow exponentially more challenging as the biological sample grows in size, and further requires reckoning with the glass transition itself, a unique multi-physics phenomenon which, at the most fundamental levels, remains mysterious [150–152]. While a complete treatment of the theory and practice of vitrification is outside the scope of this Chapter, we will here provide some salient commentary on the current state and future prospects of vitrification. We also refer the reader to several recent reviews on vitrification [73, 153, 154], and to the various other Chapters of this book that address it in varying capacities (e.g., the Chapter by Shu and colleagues, discussing the role of rewarming in vitrification, and the Chapter by Elliott and colleagues, relaying a technique for vitrification of articular cartilage).

Interplay between thermodynamics, kinetics, and transport

To achieve truly ice-free vitrification of a biological sample, the sample must travel through the metastable supercooled regime beneath its melting point and reach the safety of the glass transition temperature (at which dynamical arrest eliminates the possibility of phase change on human time scales) in a period less than the induction time of ice nucleation in the sample. As such, the success of vitrification in a given sample is a complex function of solution thermodynamics, which prescribe the distance in temperature that the sample must traverse under threat of ice formation (between the melting point and glass transition temperature); ice nucleation kinetics, which prescribe the induction time of nucleation within this distance, as a function of cooling rate; and transport, which prescribes the practitioner's ability to achieve a cooling rate that enables the sample to reach the glass transition before the according induction time. If the requirement of *total* ice avoidance is relaxed, ice *growth* kinetics also play a dominant role in this interplay, prescribing the degree to which any allowed nanoscale nucleation will develop into deleterious micro- or macro-scale ice formation. The basic logic of this interplay is laid out in **Fig. 17**, and a review of thermodynamic aspects thereof is also provided by Wowk [73].

Approaches to vitrification

This multiphysics interplay obviates many levers by which to design a successful vitrification process, and it is instructive, in contemplating directions for the development of the field, to consider each in the limit of ideal behavior.

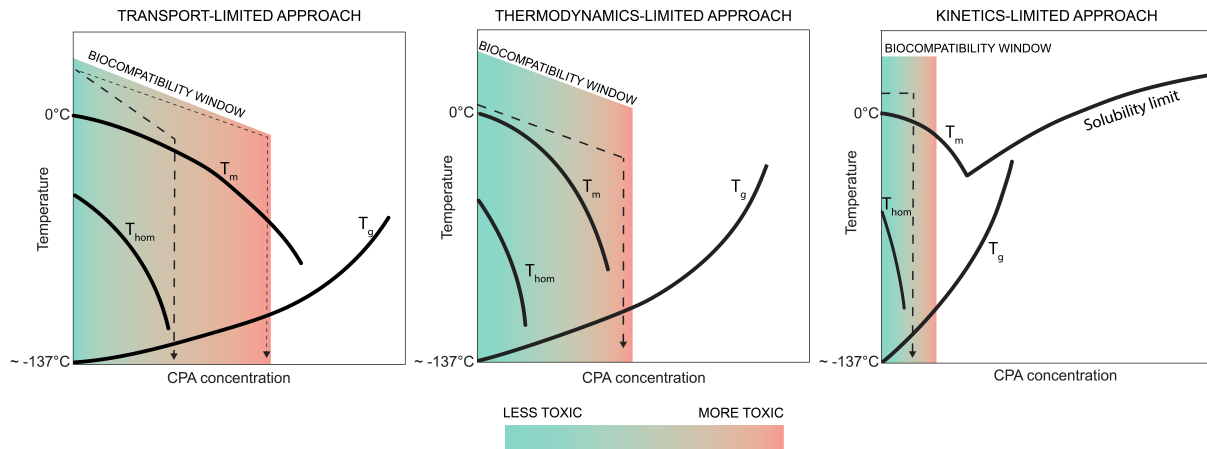


Fig. 17. In all panels, the biocompatibility window represents the range of cryoprotectant concentrations over which vitrification could be achieved with compromising the biologic through toxicity alone. The large-dashed lines represent a hypothetical temperature-concentration trajectory for a sample. T_m represents the ice-liquid melting curve; T_{hom} represents the homogeneous ice nucleation temperature, under which rate-dependent avoidance of ice is assumed practically impossible; and T_g represents the glass transition curve. Panel (a) shows the conventional transport-limited approach pioneered by Fahy and colleagues, wherein the sample is shuttled through the metastable region where ice formation is possible, but where it can be avoided by cooling and warming at sufficient speeds. Panel (b) shows a thermodynamics-limited approach, wherein novel cryoprotectants are utilized to bring the putative intersection of the melting and glass transition curves within the biocompatibility window, thereby enabling vitrification without entering a regime where ice nucleation is possible. Panel (c) shows a kinetics-limited approach, where high-molecular weight polymers or other molecules specifically suppressing the nucleation of ice (as opposed to its thermodynamic stability) are used to stabilize rate-independent passage through the metastable state. We note the role of solute solubility limits only in Panel (c), as they often prove trivially avoidable in multi-component molecular aqueous solutions, but much more challenging when polymers or large complex molecules are incorporated.

The transport-limited ideal is by far the best explored in recent literature, where it is well understood that in the limit of extremely fast cooling and warming, sensitivities of the vitrification process to the thermodynamic and kinetic parameters of the sample relax dramatically (Fig. 17, left). This concept has been richly demonstrated by Thorne and colleagues, who optimized a metallic sample holder and cryogen exposure protocol for bovine oocytes in order to achieve cooling rates up to 600,000 °C/min and warming rates up to 200,000 °C/min [155]; by Akiyama and colleagues, who developed an inkjet-based droplet extrusion platform to achieve intracellular vitrification in cells at cooling rates up to order ~1,000,000 °C/min and warming rates up to order ~10,000,000 °C/min [156]; by Bischof and colleagues, who utilized low-thermal mass, high-thermal conductivity meshes to achieve cooling and warming rates up to order ~100,000 °C/min in coral larvae, zebrafish embryos, and other small organismal samples; and in many other works reviewed in various recent papers [157]. Transport-driven vitrification techniques have also gained recent popularity in the preservation of large-scale biologics, with particular and extensive focus on new electromagnetic and photothermal interventions during the rewarming process, as surveyed in the Chapter of this book authored by Shu and colleagues.

As a brief aside, we note that curiously little effort has been applied to maximizing *cooling rates* of the same large-scale biologics, on which, as recently pointed out by Thorne and colleagues [158], measured “critical” warming rates depend. This oversight is likely a symptom of historical definitions of successful vitrification, wherein some degree of ice formation (typically ~0.2% by volume) has been accepted. In this case, wherein potentially numerous ice nuclei are allowed to form on cooling, the *growth* of those nuclei becomes asymmetrical between cooling and warming, with the vast majority occurring during warming. This asymmetry in growth in turn gives rise to the perception that the “critical” thermal rates required for successful vitrification are much larger for warming than for cooling. However, if successful vitrification is instead defined as *complete* avoidance of crystallization, critical cooling rates and warming rates become *precisely equal*, as ice nucleation is a memoryless stochastic process (i.e. agnostic to the thermal direction in which the system is moving).

The thermodynamics-limited and kinetics-limited ideals for vitrification have been investigated much more minimally. In the thermodynamic case, we may envision a biocompatible cryoprotectant solution for which the combination of melting point depression and glass transition temperature elevation together

shrink the temperature-width of the metastable zone where ice nucleation is plausible, until safe passage through this zone at achievable cooling/warming time scales becomes trivial (**Fig. 17**, middle). In the 1970s, this concept was powerfully demonstrated by Elford & Walter [69] in the cryopreservation and functional revival of cm-scale smooth muscle tissues using DMSO as the sole cryoprotectant and managing toxicity by liquidus tracking (we note that while Elford & Walter only stored the tissues at -80°C , the avoidance of ice for 24 hours at this temperature, in addition to the concentration of DMSO used, suggest that equivalent storage beneath the glass transition would also not result in freezing). However, in recent literature, and despite the exploding recent interest in vitrification of complex, multi-scale biologics, development towards (and even serious discussion of) this thermodynamic ideal has largely vanished, in favor of transport-limited strategies, pioneered by Fahy and colleagues, built around achieving “critical” cooling and warming rates needed to avoid substantial ice growth in marginally stable systems (**Fig. 17**, left). Notable exceptions to this absence are the review works of Taylor and colleagues [74, 159] and the mid-2000s research by Brockbank and colleagues on an ultra-concentrated (83% cryoprotectant by mass) derivative of the vitrification solutions developed by Fahy [160, 161]. We suggest, especially in light of recent progress in the discovery of new cryoprotectants that remain biocompatible at thermodynamically-relevant concentrations [162, 163], that this thermodynamics-limited ideal approach merits significant additional consideration.

Considering the past \sim 15 years of advances in our understanding of ice nucleation and growth processes in aqueous organic solutions, a compelling kinetics-limited ideal may also be articulated, wherein molecular or polymeric additives that interact with water and ice in increasingly *specific* ways may drive up the induction time of nucleation or inhibit post-nucleation growth, enabling ice-free cooling and warming at achievable rates in systems that retain high equilibrium melting points (**Fig. 17**, right). Ice recrystallization inhibitors, anti-freeze proteins, ice-modulating polymers [164, 165], and other agents affecting ice at the critical or sub-critical cluster scale provide promising routes to this end, especially in smaller-scale systems where the viscosities associated with high-molecular weight polymers need not preclude their use at high concentrations (as it may in vascular systems loaded by perfusion). We note further that, given the dominance of heterogeneous nucleation in vitrification of bulk (\geq mL-scale) systems, methods developed to suppress heterogeneous ice nucleation during *supercooled preservation* may be applied directly to vitrification, including elimination of air-liquid interfaces [40, 117], isolation from the atmospheric pressure reservoir via isochoric conditions [40], incorporation of ice-phobic surfaces, etc.

Toxicity, cracking, and the challenges in the vitrification of increasingly large systems

Each of the approaches described above has been demonstrated (to at least a nominal degree) in vitrification of *small* biological samples (generally pL- to uL-scale, and up to \sim 1 mL), where the intrinsically low thermal diffusivity of aqueous organic systems does not broadly prevent rapid cooling and warming; less-than-millimeter mass diffusion length scales allow effective delivery of thermodynamically-favorable cryoprotectants; and small volumes and surface areas of water within the sample minimize nucleation rates. However, in scaling to the many-mL to many-L systems relevant to organ [49, 166], whole-organism cryoconservation [167, 168], or biostasis for space travel [169], universal additional challenges emerge, including solution biocompatibility at prolonged exposure times [170], resilience against thermomechanical stress and fracture [51], and intersecting general difficulties in solution stability and deliverability.

While these problems remain far from solved, and successful vitrified cryopreservation of human-sized organs, mature organisms, etc. remains elusive, recent advances in *materials discovery* (for biocompatibility [78, 79, 163, 171]; resistance to cracking [50]; profound interaction with water [16, 172, 173]; thermal rate optimization [174, 175]; viscosity optimization [55]; etc.) offer a rapidly expanding parameter space from which to formulate optimal new vitrification protocols, according to *any* of the design principles articulated above. As such, we encourage the reader to approach their own work in vitrification with an open mind, and with consideration of the rapidly evolving physical and material bases of the field.

4 Conclusion

In this Chapter, we have sought to establish a self-consistent understanding of the physical principles driving all cryopreservation processes, in terms of a discrete set of accessible theories rooted ultimately in Gibbsian thermodynamics. We hope that the reader will carry from this work an increased appreciation of the fundamental similarities and differences between emerging cryopreservation technologies, and of the myriad opportunities to leverage these similarities and differences to hybridize, optimize, and otherwise improve their application of these technologies. We also hope that the extreme mismatch

between the potential for thermodynamic analysis in cryopreservation and the degree of analysis that has been performed will be evident, and that this mismatch will inspire ever-increasing effort in the application of thermodynamics to the pressing, impactful problems of cryobiology.

Acknowledgments

The authors acknowledge the support of the National Science Foundation (NSF) Engineering Research Center for Advanced Technologies for Preservation of Biological Systems (ATP-Bio), NSF EEC #1941543.

References

1. Tessier SN, de Vries RJ, Pendexter CA, Cronin SEJ, Ozer S, Hafiz EOA, Raigani S, Oliveira-Costa JP, Wilks BT, Lopera Higuita M, van Gulik TM, Usta OB, Stott SL, Yeh H, Yarmush ML, Uygun K, Toner M (2022) Partial freezing of rat livers extends preservation time by 5-fold. *Nat Commun* 13:4008. <https://doi.org/10.1038/s41467-022-31490-2>.
2. Maida AL, Perez PA, Bilbao-Sainz C, Rubinsky B, Consiglio AN (2025) The thermodynamic principles of isochoric freezing pressure-aided supercooling. *Cryobiology*. 118:105168. <https://doi.org/10.1016/j.cryobiol.2024.105168>
3. de Vries RJ, Tessier SN, Banik PD, Nagpal S, Cronin SEJ, Ozer S, Hafiz EOA, van Gulik TM, Yarmush ML, Markmann JF, Toner M, Yeh H, Uygun K (2019) Supercooling extends preservation time of human livers. *Nat Biotechnol* 37:1131–1136. <https://doi.org/10.1038/s41587-019-0223-y>
4. Callen HB (1985) *Thermodynamics and an introduction to thermostatistics*. Wiley, New York
5. Journaux B, Brown JM, Pakhomova A, Collings IE, Petitgirard S, Espinoza P, Boffa Ballaran T, Vance SD, Ott J, Cova F, Garbarino G, Hanfland M (2020) Holistic approach for studying planetary hydrospheres: Gibbs representation of ices thermodynamics, elasticity, and the water phase diagram to 2,300 MPa. *J Geophys Res Planets* 125:e2019JE006176. <https://doi.org/10.1029/2019JE006176>
6. Alliston SP, Dames C, Powell-Palm MJ (2025) A size-dependent ideal solution model for liquid-solid phase equilibria prediction in aqueous organic solutions. *Proc Natl Acad Sci USA* 122:e2415843122. <https://doi.org/10.1073/pnas.2415843122>
7. Flory PJ (1942) Thermodynamics of high polymer solutions. *J Chem Phys* 10:51–61. <https://doi.org/10.1063/1.1723621>
8. Hildebrand JH (1947) The entropy of solution of molecules of different size. *J Chem Phys* 15:225–228. <https://doi.org/10.1063/1.1746484>
9. Powell-Palm MJ, Smith H, Fahad MM (2024) An entropic theory of homogeneous ice nucleation in non-ionic aqueous solutions. *J Chem Phys* 160:101101. <https://doi.org/10.1063/5.0199398>
10. Elliott JAW, Prickett RC, Elmoazzen HY, Porter KR, McGann LE (2007) A multisolute osmotic virial equation for solutions of interest in biology. *J Phys Chem B* 111:1775–1785. <https://doi.org/10.1021/jp0680342>
11. Prickett RC, Elliott JAW, McGann LE (2010) Application of the osmotic virial equation in cryobiology. *Cryobiology* 60:30–42. <https://doi.org/10.1016/j.cryobiol.2009.07.011>
12. Prickett RC, Elliott JAW, McGann LE (2011) Application of the multisolute osmotic virial equation to solutions containing electrolytes. *J Phys Chem B* 115:14531–14543. <https://doi.org/10.1021/jp206011m>
13. Prausnitz JM, Lichtenhaller RN, De Azevedo EG (1999) *Molecular thermodynamics of fluid-phase equilibria*. Prentice Hall PTR
14. Ganbavale G, Zuend A, Marcolli C, Peter T (2015) Improved AIOMFAC model parameterisation of the temperature dependence of activity coefficients for aqueous organic mixtures. *Atmos Chem Phys* 15:447–493. <https://doi.org/10.5194/acp-15-447-2015>
15. Eckert F, Klamt A (2002) Fast solvent screening via quantum chemistry: COSMO-RS approach. *AIChE J* 48:369–385. <https://doi.org/10.1002/aic.690480220>
16. Mallya AS, Yadav P, Zakhia S, Hubel A (2025) Computational design of natural deep eutectic systems using COSMO-RS for ice control applications. *ACS Sustain Chem Eng* 13:14683–14692. <https://doi.org/10.1021/acssuschemeng.5c01597>
17. Bell IH, Mickoleit E, Hsieh CM, Lin ST, Vrabec J, Breitkopf C, Jäger A (2020) A benchmark open-source implementation of COSMO-SAC. *J Chem Theory Comput* 16:2635–2646. <https://doi.org/10.1021/acs.jctc.9b01016>
18. Rubinsky B, Perez PA, Carlson ME (2005) The thermodynamic principles of isochoric cryopreservation. *Cryobiology* 50:121–138. <https://doi.org/10.1016/j.cryobiol.2004.12.002>
19. Consiglio AN, Rubinsky B, Powell-Palm MJ (2024) A review of the physical principles of isochoric cryopreservation. *Annu Rev Heat Transfer* 27:93–164. <https://doi.org/10.1615/AnnualRevHeatTransfer.2024054596>
20. Powell-Palm MJ (2022) Calculation of a temperature-volume phase diagram of water to inform the study of isochoric freezing down to cryogenic temperatures. *RSC Adv* 12:20603–20609. <https://doi.org/10.1039/D2RA03683E>

21. Mazur P, Leibo SP, Chu EHY (1972) A two-factor hypothesis of freezing injury: evidence from Chinese hamster tissue-culture cells. *Exp Cell Res* 71:345–355. [https://doi.org/10.1016/0014-4827\(72\)90303-5](https://doi.org/10.1016/0014-4827(72)90303-5)
22. Sutton RL (1991) Critical cooling rates to avoid ice crystallization in aqueous cryoprotectant solutions containing polymers. *J Chem Soc Faraday Trans* 87:3747–3751. <https://doi.org/10.1039/FT9918703747>
23. Hobbs PV (2010) *Ice physics*. Oxford University Press, New York
24. Blazquez S, Sanz E (2025) On the growth rate of ices: effect of pressure and ice phase. *J Chem Phys* 162:194501. <https://doi.org/10.1063/5.0265605>
25. Toner M, Cravalho EG, Karel M (1990) Thermodynamics and kinetics of intracellular ice formation during freezing of biological cells. *J Appl Phys* 67:1582–1593. <https://doi.org/10.1063/1.345670>
26. Nada H, Furukawa Y (2012) Antifreeze proteins: computer simulation studies on the mechanism of ice growth inhibition. *Polym J* 44:690–698. <https://doi.org/10.1038/pj.2012.13>
27. Meister K, Devries AL, Bakker HJ, Drori R (2018) Antifreeze glycoproteins bind irreversibly to ice. *J Am Chem Soc* 140:9365–9368. <https://doi.org/10.1021/jacs.8b04966>
28. Biggs CI, Bailey TL, Ben Graham, Stubbs C, Fayter A, Gibson MI (2017) Polymer mimics of biomacromolecular antifreezes. *Nat Commun* 8:1546. <https://doi.org/10.1038/s41467-017-01421-7>
29. Budke C, Koop T (2006) Ice recrystallization inhibition and molecular recognition of ice faces by poly(vinyl alcohol). *Chem Phys Chem* 7:2601–2606. <https://doi.org/10.1002/cphc.200600533>
30. Pruppacher HR, Klett JD (2010) *Microphysics of clouds and precipitation*. Springer Netherlands.
31. Barahona D (2018) On the thermodynamic and kinetic aspects of immersion ice nucleation. *Atmos Chem Phys* 18:17119–17141. <https://doi.org/10.5194/acp-18-17119-2018>
32. Consiglio AN, Ouyang Y, Powell-Palm MJ, Rubinsky B (2023) An extreme value statistics model of heterogeneous ice nucleation for quantifying the stability of supercooled aqueous systems. *J Chem Phys* 159:064511. <https://doi.org/10.1063/5.0155494>
33. Barahona D (2014) Analysis of the effect of water activity on ice formation using a new thermodynamic framework. *Atmos Chem Phys* 14:7665–7680. <https://doi.org/10.5194/acp-14-7665-2014>
34. Barahona D (2015) Thermodynamic derivation of the activation energy for ice nucleation. *Atmos Chem Phys* 15:13819–13831. <https://doi.org/10.5194/acp-15-13819-2015>
35. Koop T, Luo B, Biermann UM, Crutzen PJ, Peter T (1997) Freezing of HNO₃/H₂SO₄/H₂O solutions at stratospheric temperatures: nucleation statistics and experiments. *J Phys Chem A* 101:1117–1133. <https://doi.org/10.1021/jp9626531>
36. Liu Y, He L, Zhao G (2025) Multiscale heat and mass transfer in biomaterial cryopreservation. *Int J Heat Mass Transf* 252:127414. <https://doi.org/10.1016/j.ijheatmasstransfer.2025.127414>
37. Guo Z, Zhan L, Finger EB, Hays TS, Toner M, Bischof JC (2024) Enhanced heat transfer for improved ice-free cryopreservation – Interplay between cooling and rewarming. *Annu Rev Heat Transfer* 27:195–244. <https://doi.org/10.1615/AnnualRevHeatTransfer.2024054907>
38. Fahy GM, MacFarlane DR, Angell CA, Meryman HT (1984) Vitrification as an approach to cryopreservation. *Cryobiology* 21:407–426. [https://doi.org/10.1016/0011-2240\(84\)90079-8](https://doi.org/10.1016/0011-2240(84)90079-8)
39. Ashrafi E, Elliott JAW (2025) Interrupted cooling protocols in cryopreservation: a review of fundamentals, methods and experimental outcomes for cells in suspension. *Cryobiology* 121:105339. <https://doi.org/10.1016/j.cryobiol.2025.105339>
40. Consiglio AN, Lilley D, Prasher R, Rubinsky B, Powell-Palm MJ (2022) Methods to stabilize aqueous supercooling identified by use of an isochoric nucleation detection (INDe) device. *Cryobiology* 106:91–101. <https://doi.org/10.1016/j.cryobiol.2022.03.003>
41. Gillooly JF, Brown JH, West GB, Savage VM, Charnov EL (2001) Effects of size and temperature on metabolic rate. *Science* 293:2248–2251. <https://doi.org/10.1126/science.1061967>
42. Consiglio AN, Rubinsky B, Powell-Palm MJ (2022) Relating metabolism suppression and nucleation probability during supercooled biopreservation. *J Biomech Eng* 144:144:074504. <https://doi.org/10.1115/1.4054217>
43. Benson JD, Higgins AZ, Desai K, Eroglu A (2018) A toxicity cost function approach to optimal CPA equilibration in tissues. *Cryobiology* 80:144–155. <https://doi.org/10.1016/j.cryobiol.2017.09.005>
44. Olver DJ, Heres P, Paredes E, Benson JD (2023) Rational synthesis of total damage during cryoprotectant equilibration: modelling and experimental validation of osmomechanical, temperature, and cytotoxic damage in sea urchin (*Paracentrotus lividus*) oocytes. *PeerJ* 9:e15539. <https://doi.org/10.7717/peerj.15539>
45. Warner RM, Brown KS, Benson JD, Eroglu A, Higgins AZ (2022) Multiple cryoprotectant toxicity model for vitrification solution optimization. *Cryobiology* 108:1–9. <https://doi.org/10.1016/j.cryobiol.2022.09.002>
46. Rubinsky B, Cravalho EG, Mikic B (1980) Thermal stresses in frozen organs. *Cryobiology* 17:66–73. [https://doi.org/10.1016/0011-2240\(80\)90009-7](https://doi.org/10.1016/0011-2240(80)90009-7)
47. Shaw JM, Kuleshova LL, MacFarlane DR, Trounson AO (1997) Vitrification properties of solutions of ethylene glycol in saline containing PVP, Ficoll, or dextran. *Cryobiology* 35:219–229. <https://doi.org/10.1006/cryo.1997.2043>
48. Ehrlich LE, Fahy GM, Wowk BG, Malen JA, Rabin Y (2018) Thermal analyses of a human kidney and a rabbit kidney during cryopreservation by vitrification. *J Biomech Eng* 140:0110051–0110058. <https://doi.org/10.1115/1.4037406>

49. Han Z, Rao JS, Gangwar L, Namsrai BE, Pasek-Allen JL, Etheridge ML, Wolf SM, Pruitt TL, Bischof JC, Finger EB (2023) Vitrification and nanowarming enable long-term organ cryopreservation and life-sustaining kidney transplantation in a rat model. *Nat Commun* 14:3407. <https://doi.org/10.1038/s41467-023-38824-8>
50. Kavian S, Sellers R, Sanchez GA, Alvarez C, Aguilar G, Powell-Palm MJ (2025) Higher glass transition temperatures reduce thermal stress cracking in aqueous solutions relevant to cryopreservation. *Sci Rep* 15:27903. <https://doi.org/10.1038/s41598-025-13295-7>
51. Rabin Y (2024) Thermomechanics modeling and visualization of physical effects to improve cryopreservation by vitrification. *Annu Rev Heat Transfer* 27:245–282. <https://doi.org/10.1615/AnnualRevHeatTransfer.2024053892>
52. Solanki PK, Rabin Y (2022) Perspective: Temperature-dependent density and thermal expansion of cryoprotective agents. *CryoLetters* 43:1–9. <https://doi.org/10.54680/fr2211011012>
53. Noday DA, Steif PS, Rabin Y (2009) Viscosity of cryoprotective agents near glass transition: a new device, technique, and data on DMSO, DP6, and VS55. *Exp Mech* 49:663–672. <https://doi.org/10.1007/s11340-008-9191-8>
54. Han Z, Bischof JC (2020) Critical cooling and warming rates as a function of CPA concentration. *CryoLetters* 41:185–193
55. Kavian S, Zarriz A, Powell-Palm MJ (2025) Physics-informed neural networks for predicting viscosity of many-component organic and aqueous solutions. <https://doi.org/10.2139/ssrn.5649193>
56. Zarriz A, Journaux B, Powell-Palm MJ (2024) On the equilibrium limit of liquid stability in pressurized aqueous systems. *Nature Commun* 15:10666. <https://doi.org/10.1038/s41467-024-54625-z>
57. Chang B, Consiglio AN, Lilley D, Prasher R, Rubinsky B, Journaux B, Powell-Palm MJ (2022) On the pressure dependence of salty aqueous eutectics. *Cell Rep Phys Sci* 3:100856. <https://doi.org/10.1016/j.xcrp.2022.100856>
58. Karlsson JOM, Cravalho EG, Toner M (1994) A model of diffusion-limited ice growth inside biological cells during freezing. *J Appl Phys* 75:4442–4455. <https://doi.org/10.1063/1.355959>
59. Shardt N, Chen Z, Yuan SC, Wu K, Laouar L, Jomha NM, Elliott JAW (2020) Using engineering models to shorten cryoprotectant loading time for the vitrification of articular cartilage. *Cryobiology* 92:180–188. <https://doi.org/10.1016/j.cryobiol.2020.01.008>
60. Kangas J, Hogan CJ (2024) Mathematical treatments of ice formation and vitrification during cryopreservation. *Annu Rev Heat Transfer* 27:25–69. <https://doi.org/10.1615/AnnualRevHeatTransfer.2024053903>
61. Boutron P (1986) Comparison with the theory of the kinetics and extent of ice crystallization and of the glass-forming tendency in aqueous cryoprotective solutions. *Cryobiology* 23:88–102. [https://doi.org/10.1016/0011-2240\(86\)90022-2](https://doi.org/10.1016/0011-2240(86)90022-2)
62. Murray BJ (2008) Inhibition of ice crystallisation in highly viscous aqueous organic acid droplets. *Atmos Chem Phys* 8:5423–5433. <https://doi.org/10.5194/acp-8-5423-2008>
63. Bronshteyn VL, Steponkus PL (1995) Nucleation and growth of ice crystals in concentrated solutions of ethylene glycol. *Cryobiology* 32:1–22. <https://doi.org/10.1006/cryo.1995.1001>
64. Hey JM, Macfarlane DR (1996) Crystallization of ice in aqueous solutions of glycerol and dimethyl sulfoxide. 1. A comparison of mechanisms. *Cryobiology* 33:205–216. <https://doi.org/10.1006/cryo.1996.0021>
65. Hey JM, MacFarlane DR (1998) Crystallization of ice in aqueous solutions of glycerol and dimethyl sulfoxide 2: Ice crystal growth kinetics. *Cryobiology* 37:119–130. <https://doi.org/10.1006/cryo.1998.2108>
66. Sei T, Gonda T, Arima Y (2002) Growth rate and morphology of ice crystals growing in a solution of trehalose and water. *J Cryst Growth* 240:218–229. [https://doi.org/10.1016/S0022-0248\(02\)00875-8](https://doi.org/10.1016/S0022-0248(02)00875-8)
67. Vigier G, Thollet G, Vassouille R (1987) Cubic and hexagonal ice formation in water-glycerol mixture (50% w/w). *J Cryst Growth* 84:309–315. [https://doi.org/10.1016/0022-0248\(87\)90146-1](https://doi.org/10.1016/0022-0248(87)90146-1)
68. Farrant J (1965) Mechanism of cell damage during freezing and thawing and its prevention. *Nature* 205:1284–1287. <https://doi.org/10.1038/2051284a0>
69. Elford BC, Walter CA (1972) Preservation of structure and function of smooth muscle cooled to -79 °C in unfrozen aqueous media. *Nature New Biol* 236:58–60. <https://doi.org/10.1038/newbio236058a0>
70. Pegg DE, Wang L, Vaughan D (2006) Cryopreservation of articular cartilage. Part 3: the liquidus-tracking method. *Cryobiology* 52:360–368. <https://doi.org/10.1016/j.cryobiol.2020.01.004>
71. Kay AG, Hoyland JA, Rooney P, Kearney JN, Pegg DE (2015) A liquidus tracking approach to the cryopreservation of human cartilage allografts. *Cryobiology* 71:77–84. <https://doi.org/10.1016/j.cryobiol.2015.05.005>
72. Puschmann E, Selden C, Butler S, Fuller B (2017) Liquidus tracking: large scale preservation of encapsulated 3-D cell cultures using a vitrification machine. *Cryobiology* 76:65–73. <https://doi.org/10.1016/j.cryobiol.2017.04.006>
73. Wowk B (2010) Thermodynamic aspects of vitrification. *Cryobiology* 60:11–22. <https://doi.org/10.1016/j.cryobiol.2009.05.007>
74. Taylor MJ, Weegman BP, Baicu SC, Giwa SE (2019) New approaches to cryopreservation of cells, tissues, and organs. *Transfus Med Hemother* 46:197–215. <https://doi.org/10.1159/000499453>
75. Berendsen TA, Bruinsma BG, Puts CF, Saeidi N, Usta OB, Uygun BE, Izamis ML, Toner M, Yarmush ML, Uygun K (2014) Supercooling enables long-term transplantation survival following 4 days of liver preservation. *Nat Med* 20:790–793. <https://doi.org/10.1038/nm.3588>

76. Botea F, Năstase G, Herlea V, Chang TT, Ţerban A, Barcu A, Rubinsky B, Popescu I (2023) An exploratory study on isochoric supercooling preservation of the pig liver. *Biochem Biophys Rep* 34:101485. <https://doi.org/10.1016/j.bbrep.2023.101485>

77. Fawad M, Elde S, Heng E, Krishnan A, Consiglio AN, Vergel M, Alnasir D, Choi A, Simmons J, MacArthur J, Shudo Y, Ruaengsri C, Woo J, Powell-Palm MJ, Guenthart B (2025) First sub-zero cardiac allograft preservation and reanimation following 24-hours of isochoric supercooled preservation. *J Heart Lung Transplantat* 44:S36. <https://doi.org/10.1016/j.healun.2025.02.080>

78. Ahmadkhani N, Benson JD, Eroglu A, Higgins AZ (2025) High throughput method for simultaneous screening of membrane permeability and toxicity for discovery of new cryoprotective agents. *Sci Rep* 15: 1862. <https://doi.org/10.1038/s41598-025-85509-x>

79. Ahmadkhani N, Sugden C, Mayo AT, Higgins AZ (2025) Screening for cryoprotective agent toxicity and toxicity reduction in mixtures at subambient temperatures. *Cryobiology* 121:105315. <https://doi.org/10.1016/j.cryobiol.2025.105315>

80. Ishine N, Rubinsky B, Lee CY (1999) A histological analysis of liver injury in freezing storage. *Cryobiology* 39:271–277. <https://doi.org/10.1006/cryo.1999.2205>

81. Ishine N, Rubinsky B, Lee CY (2000) Transplantation of mammalian livers following freezing: vascular damage and functional recovery. *Cryobiology* 40:84–89. <https://doi.org/10.1006/cryo.1999.2225>

82. Tessier SN, de Vries RJ, Pendexter CA, Cronin SEJ, Ozer S, Hafiz EOA, Raigani S, Oliveira-Costa JP, Wilks BT, Lopera Higuita M, van Gulik TM, Usta OB, Stott SL, Yeh H, Yarmush ML, Uygun K, Toner M (2022) Partial freezing of rat livers extends preservation time by 5-fold. *Nat Commun* 13:4008. <https://doi.org/10.1038/s41467-022-31490-2>

83. Tessier SN, Haque O, Pendexter CA, Cronin SEJ, Hafiz EOA, Weng L, Yeh H, Markmann JF, Taylor MJ, Fahy GM, Toner M, Uygun K (2022) The role of antifreeze glycoprotein (AFGP) and polyvinyl alcohol/polyglycerol (X/Z-1000) as ice modulators during partial freezing of rat livers. *Front Phys* 10:1033613. <https://doi.org/10.3389/fphy.2022.1033613>

84. Ozgur OS, Taggart M, Mojoudi M, Pendexter C, Filz von Reiterdank I, Kharga A, Yeh H, Toner M, Longchamp A, Tessier SN, Uygun K (2024) Optimized partial freezing protocol enables 10-day storage of rat livers. *Sci Rep* 14:25260. <https://doi.org/10.1038/s41598-024-76674-6>

85. Taggart M, Hassan M, Ozgur O, Lyon A, Mojoudi M, Cutrone A, Taveras C, Toner M, Tessier S, Markmann J, Yeh H, Longchamp A, Uygun K (2025) Preservation of discarded human kidneys for 10 days at subzero temperature. *Am J Transplant* 25:S14–S15. <https://doi.org/10.1016/j.ajt.2024.12.035>

86. Lyu C, Luo G, An R, Wang D, Rubinsky B (2024) Inactivation of *Bacillus cereus* spores by isochoric freezing. *Food Control* 161:110383. <https://doi.org/10.1016/j.foodcont.2024.110383>

87. Wan L, Powell-Palm MJ, Lee C, Gupta A, Weegman BP, Clemens MG, Rubinsky B (2018) Preservation of rat hearts in subfreezing temperature isochoric conditions to -8°C and 78 MPa. *Biochem Biophys Res Commun* 496:852–857. <https://doi.org/10.1016/j.bbrc.2018.01.140>

88. Wan L, Powell-Palm MJ, Clemens MG, Rubinsky B (2019) Time-dependent effects of pressure during preservation of rat hearts in an isochoric system at subfreezing temperatures. *CryoLetters* 40:64–70

89. Zielinski MW, McGann LE, Nychka JA, Elliott JAW (2014) Comparison of non-ideal solution theories for multi-solute solutions in cryobiology and tabulation of required coefficients. *Cryobiology* 69:305–317. <https://doi.org/10.1016/j.cryobiol.2014.08.005>

90. Wang SC, Wang CK, Chang FM, Tsao HK (2002) Second virial coefficients of poly(ethylene glycol) in aqueous solutions at freezing point. *Macromolecules* 35:9551–9555. <https://doi.org/10.1021/ma025663a>

91. Kim Y, Goswami I, Gill E, Mahmoodi SR, Consiglio AN, Velazquez J, Nieman G, Alburo AAA, Woods B, Ellis BW, Filz von Reiterdank I, Uygun K, Uygun BE, Rubinsky B, Healy KE (2025) Vascular microphysiological system for investigating endothelial barrier function during organ preservation and reperfusion. *Small* 21:e2410168. <https://doi.org/10.1002/smll.202410168>

92. Kapanen MK, Halavaara JT, Häkkinen AM (2005) Open Four-Compartment Model in the Measurement of liver Perfusion. *Acad Radiol* 12:1542–1550. <https://doi.org/10.1016/j.acra.2005.07.001>

93. Morris GJ, Acton E (2013) Controlled ice nucleation in cryopreservation - a review. *Cryobiology* 66:85–92. <https://doi.org/10.1016/j.cryobiol.2012.11.007>

94. He Z, Liu K, Wang J (2018) Bioinspired materials for controlling ice nucleation, growth, and recrystallization. *Acc Chem Res* 51:1082–1091. <https://doi.org/10.1021/acs.accounts.7b00528>

95. Zhang Z, Liu XY (2018) Control of ice nucleation: freezing and antifreeze strategies. *Chem Soc Rev* 47:7116–7139. <https://doi.org/10.1039/c8cs00626a>

96. Harrison AD, Whale TF, Carpenter MA, Holden MA, Neve L, O'Sullivan D, Vergara Temprado J, Murray BJ (2016) Not all feldspars are equal: a survey of ice nucleating properties across the feldspar group of minerals. *Atmos Chem Phys* 16:10927–10940. <https://doi.org/10.5194/acp-16-10927-2016>

97. Murray KA, Kinney NLH, Griffiths CA, Hasan M, Gibson MI, Whale TF (2022) Pollen derived macromolecules serve as a new class of ice-nucleating cryoprotectants. *Sci Rep* 12:12295. <https://doi.org/10.1038/s41598-022-15545-4>

98. Sosso GC, Whale TF, Holden MA, Pedevilla P, Murray BJ, Michaelides A (2018) Unravelling the origins of ice nucleation on organic crystals. *Chem Sci* 9:8077–8088. <https://doi.org/10.1039/c8sc02753f>

99. Failor KC, Schmale DG 3rd, Vinatzer BA, Monteil CL (2017) Ice nucleation active bacteria in precipitation are genetically diverse and nucleate ice by employing different mechanisms. *ISME J* 11:2740–2753. <https://doi.org/10.1038/ismej.2017.124>
100. Consiglio A, Ukpai G, Rubinsky B, Powell-Palm MJ (2020) Suppression of cavitation-induced nucleation in systems under isochoric confinement. *Phys Rev Research* 2:023350. <https://doi.org/10.1103/PhysRevResearch.2.023350>
101. Peng Z, Li W, Liu B, Wang J (2025) Ultrasonic ice seeding as an effective technique for Hep-G2 cell cryopreservation. *CryoLetters* 46:345–354. <https://doi.org/10.54680/fr25510110412>
102. Tian Y, Zhang P, Zhu Z, Sun DW (2020) Development of a single/dual-frequency orthogonal ultrasound-assisted rapid freezing technique and its effects on quality attributes of frozen potatoes. *J Food Eng* 286:110112. <https://doi.org/10.1016/j.jfoodeng.2020.110112>
103. Alcalá E, Encabo L, Barroso F, Puentes A, Risco I, Risco R (2023) Sound waves for solving the problem of recrystallization in cryopreservation. *Sci Rep* 13:7603. <https://doi.org/10.1038/s41598-023-34681-z>
104. Franks F, Wakabayashi T, Mathias SF (1987) Nucleation kinetics of ice in undercooled yeast cells: long-term stability against freezing. *Microbiology* 133:2807–2815. <https://doi.org/10.1099/00221287-133-10-2807>
105. Barnes BM (1989) Freeze avoidance in a mammal: body temperatures below 0°C in an arctic hibernator. *Science* 244:1593–1595. <https://doi.org/10.1126/science.2740905>
106. Usta OB, Kim Y, Ozer S, Bruinsma BG, Lee J, Demir E, Berendsen TA, Puts CF, Izamis ML, Uygun K, Uygun BE, Yarmush ML (2013) Supercooling as a viable non-freezing cell preservation method of rat hepatocytes. *PLoS One* 8:e69334. <https://doi.org/10.1371/journal.pone.0069334>
107. Powell-Palm MJ, Charwat V, Charrez B, Siemons B, Healy KE, Rubinsky B (2021) Isochoric supercooled preservation and revival of human cardiac microtissues. *Commun Biol* 4:1118. <https://doi.org/10.1038/s42003-021-02650-9>
108. Berkane Y, Filz von Reiterdank I, Tawa P, Charlès L, Goutard M, Dinicu AT, Toner M, Bertheuil N, Mink van der Molen AB, Coert JH, Lellouch AG, Randolph MA, Cetrulo CL Jr, Uygun K (2024) VCA supercooling in a swine partial hindlimb model. *Sci Rep* 14:12618. <https://doi.org/10.1038/s41598-024-63041-8>
109. Jiao X, Li Y, Chen Z, Zhang Q, He R, Huang Y, Zuo Z (2024) Targeting the PDE3B-cAMP-autophagy axis prevents liver injury in long-term supercooling liver preservation. *Sci Transl Med* 16:eadk0636. <https://doi.org/10.1126/scitranslmed.adk0636>
110. Isiksacan Z, William N, Senturk R, Boudreau L, Wooning C, Castellanos E, Isiksacan S, Yarmush ML, Acker JP, Usta OB (2024) Extended supercooled storage of red blood cells. *Commun Biol* 7:765. <https://doi.org/10.1038/s42003-024-06463-4>
111. Puts CF, Berendsen TA, Bruinsma BG, Ozer S, Luitje M, Usta OB, Yarmush ML, Uygun K (2015) Polyethylene glycol protects primary hepatocytes during supercooling preservation. *Cryobiology* 71:125–129. <https://doi.org/10.1016/j.cryobiol.2015.04.010>
112. Isiksacan Z, William N, Yarmush ML, Acker JP, Usta OB (2023) Long-term preservation of red blood cells through deep supercooling. *Cryobiology* 113:104654. <https://doi.org/10.1016/j.cryobiol.2023.104654>
113. Huang H, Rey-Bedón C, Yarmush ML, Usta OB (2020) Deep-supercooling for extended preservation of adipose-derived stem cells. *Cryobiology* 92:67–75. <https://doi.org/10.1016/j.cryobiol.2019.11.004>
114. William N, Isiksacan Z, Mykhailova O, Olafson C, Yarmush ML, Usta OB, Acker JP (2023) Comparing two extracellular additives to facilitate extended storage of red blood cells in a supercooled state. *Front Physiol* 14:1165330. <https://doi.org/10.3389/fphys.2023.1165330>
115. Li Y, Li Z, Peng L, Huang H (2025) Deep-supercooling preservation for rat kidneys. *Transplantation*, <https://doi.org/10.1097/TP.0000000000005550>
116. Huang H, Yarmush ML, Usta OB (2018) Long-term deep-supercooling of large-volume water and red cell suspensions via surface sealing with immiscible liquids. *Nat Commun* 9:3201. <https://doi.org/10.1038/s41467-018-05636-0>
117. Powell-Palm MJ, Koh-Bell A, Rubinsky B (2020) Isochoric conditions enhance stability of metastable supercooled water. *Appl Phys Lett* 116:123702. <https://doi.org/10.1063/1.5145334>
118. Wang L, Meng H, Wang F, Liu H (2024) Ice nucleation mechanisms and the maintenance of supercooling in water under mechanical vibration. *Results Phys* 59:107581. <https://doi.org/10.1016/j.rinp.2024.107581>
119. Powell-Palm MJ, Rubinsky B, Sun W (2020) Freezing water at constant volume and under confinement. *Commun Phys* 3:39. <https://doi.org/10.1038/s42005-020-0303-9>
120. Kimizuka N, Viriyattanakorn C, Suzuki T (2008) Ice nucleation and supercooling behavior of polymer aqueous solutions. *Cryobiology* 56:80–87. <https://doi.org/10.1016/j.cryobiol.2007.10.179>
121. Zobrist B, Weers U, Koop T (2003) Ice nucleation in aqueous solutions of poly[ethylene glycol] with different molar mass. *J Chem Phys* 118:10254–10261. <https://doi.org/10.1063/1.1571818>
122. Bardsley WE, Khatep MM (1984) A general model for temperature of heterogeneous nucleation of supercooled water droplets. *J Atm Sci* 41:856–862. [https://doi.org/10.1175/1520-0469\(1984\)041<0856:AGMFTO>2.0.CO;2](https://doi.org/10.1175/1520-0469(1984)041<0856:AGMFTO>2.0.CO;2)
123. Langham EJ, Mason BJ (1958) The heterogeneous and homogeneous nucleation of supercooled water. *Proc R Soc Lond A Math Phys Sci* 247:493–504. <https://doi.org/10.1098/rspa.1958.0207>

124. Deck LT, Wittenberg L, Mazzotti M (2023) Thermodynamics explains how solution composition affects the kinetics of stochastic ice nucleation. *J Phys Chem Lett* 14:5993–6000. <https://doi.org/10.1021/acs.jpclett.3c01371>

125. Song F, Sato M, Toyama Y, Tokito F, Katsuda T, Toyooka K, Sakai Y, Nishikawa M (2025) A proof-of-concept study on high pressure freezing for cryopreservation. *PNAS Nexus* (in press).

126. Han HM, Huebinger J, Grabenbauer M (2012) Self-pressurized rapid freezing (SPRF) as a simple fixation method for cryo-electron microscopy of vitreous sections. *J Struct Biol* 178:84–87. <https://doi.org/10.1016/j.jsb.2012.04.001>

127. Grabenbauer M, Han HM, Huebinger J (2014) Cryo-fixation by self-pressurized rapid freezing. In: Kuo (ed), *Electron microscopy, Methods in Molecular Biology*, Humana Press, Totowa, NJ, 173–191. https://doi.org/10.1007/978-1-62703-776-1_9

128. Rubinsky B, Ikeda M (1985) A cryomicroscope using directional solidification for the controlled freezing of biological material. *Cryobiology* 22:55–68. [https://doi.org/10.1016/0011-2240\(85\)90008-2](https://doi.org/10.1016/0011-2240(85)90008-2)

129. Upkai G, Rubinsky B (2020) A mathematical analysis of directional solidification of aqueous solutions. *J Heat Transfer* 142:022401. <https://doi.org/10.1115/1.4045312>

130. Bahari L, Bein A, Yashunsky V, Braslavsky I (2018) Directional freezing for the cryopreservation of adherent mammalian cells on a substrate. *PLoS One* 13:e0192265. <https://doi.org/10.1371/journal.pone.0192265>

131. Saragusty J (2015) Directional freezing for large volume cryopreservation. In: Wolkers, W., Oldenhof, H. (eds) *Cryopreservation and freeze-drying protocols, Methods in Molecular Biology* 1257. Springer, New York, NY, 381–397. https://doi.org/10.1007/978-1-4939-2193-5_19

132. Si W, Hildebrandt TB, Reid C, Krieg R, Ji W, Fassbender M, Hermes R (2006) The successful double cryopreservation of rabbit (*Oryctolagus cuniculus*) semen in large volume using the directional freezing technique with reduced concentration of cryoprotectant. *Theriogenology* 65:788–798. <https://doi.org/10.1016/j.theriogenology.2005.06.010>

133. Si W, Lu Y, He X, Ji S, Niu Y, Tan T, Ji W (2010) Directional freezing as an alternative method for cryopreserving rhesus macaque (*Macaca mulatta*) sperm. *Theriogenology* 74:1431–1438. <https://doi.org/10.1016/j.theriogenology.2010.06.015>

134. O'Brien JK, Robeck TR (2010) Preservation of beluga (*Delphinapterus leucas*) spermatozoa using a trehalose-based cryodiluent and directional freezing technology. *Reprod Fertil Dev* 22, 653–663 (2010). <https://doi.org/10.1071/RD09176>

135. Arav A (1996) Device and methods for multigradient directional cooling and warming of biological samples. U.S. Patent No. 5,873,254.

136. Revel A, Elami A, Bor A, Yavin S, Natan Y, Arav A (2004) Whole sheep ovary cryopreservation and transplantation. *Fertil Steril* 82:1714–1715. <https://doi.org/10.1016/j.fertnstert.2004.06.046>

137. Arav A, Revel A, Nathan Y, Bor A, Gacitua H, Yavin S, Gavish Z, Uri M, Elami A (2005) Oocyte recovery, embryo development and ovarian function after cryopreservation and transplantation of whole sheep ovary. *Hum Reprod* 20:3554–3559. <https://doi.org/10.1093/humrep/dei278>

138. Maffei S, Pennarossa G, Brevini TA, Arav A, Gandolfi F (2014) Beneficial effect of directional freezing on in vitro viability of cryopreserved sheep whole ovaries and ovarian cortical slices. *Hum Reprod* 29:114–124. <https://doi.org/10.1093/humrep/det377>

139. Birdseye C (1927) Method of preparing food products. U.S. Patent No. 1,773,079

140. Sun D (2013) *Handbook of frozen food processing and packaging food oral processing: fundamentals of eating and sensory perception*. Taylor & Francis

141. Jiang L, Liu D, Wang W, Lv R, Yu S, Zhou J (2025) Advancements and perspectives of novel freezing and thawing technologies effects on meat: a review. *Food Res Int* 204:115942. <https://doi.org/10.1016/j.foodres.2025.115942>

142. Loayza-Salazar S, Siche R, Vegas C, Chávez-Llerena RT, Encina-Zelada CR, Calla-Florez M, Comettant-Rabanal R (2024) Novel technologies in the freezing process and their impact on the quality of fruits and vegetables. *Food Eng Rev* 16:371–395. <https://doi.org/10.1007/s12393-024-09371-9>

143. Salvadori VO, Mascheroni RH (2002) Analysis of impingement freezers performance. *J Food Eng* 54:133–140. [https://doi.org/10.1016/S0260-8774\(01\)00198-4](https://doi.org/10.1016/S0260-8774(01)00198-4)

144. James C, Purnell G, James SJ (2015) A review of novel and innovative food freezing technologies. *Food Bioproc Tech* 8:1616–1634. <https://doi.org/10.1007/s11947-015-1542-8>

145. Akiyama Y, Shinose M, Watanabe H, Yamada S, Kanda Y (2019) Cryoprotectant-free cryopreservation of mammalian cells by superflash freezing. *Proc Natl Acad Sci USA* 116:7738–7743. <https://doi.org/10.1073/pnas.1808645116>

146. Yu Z, Garcia AS, Johnston KP, Williams RO (2004) Spray freezing into liquid nitrogen for highly stable protein nanostructured microparticles. *Eur J Pharm Biopharm* 58:529–537. <https://doi.org/10.1016/j.ejpb.2004.04.018>

147. Zhou X, Liu Z, Liang XM, Shu Z, Du P, Gao D (2013) Theoretical investigations of a novel microfluidic cooling/warming system for cell vitrification cryopreservation. *Int J Heat Mass Transf* 65, 381–388. <https://doi.org/10.1016/j.ijheatmasstransfer.2013.06.022>

148. Shi M, Ling K, Yong KW, Li Y, Feng S, Zhang X, Pingguan-Murphy B, Lu TJ, Xu F (2015) High-throughput non-contact vitrification of cell-laden droplets based on cell printing. *Sci Rep* 5:17928. <https://doi.org/10.1038/srep17928>

149. Luyet BJ, Hodapp EL (1938) Revival of frog's spermatozoa vitrified in liquid air. *Proc Soc Exp Biol Med* 39:433–434. <https://doi.org/10.3181/00379727-39-10229P>
150. Berthier L, Reichman DR (2023) Modern computational studies of the glass transition. *Nat Rev Phys* 5:102–116. <https://doi.org/10.1038/s42254-022-00548-x>
151. Kivelson SA, Tarjus G (2008) In search of a theory of supercooled liquids. *Nat Mater* 7:831–833. <https://doi.org/10.1038/nmat2304>
152. Lunkenheimer P, Loidl A, Riechers B, Zaccione A, Samwer K (2023) Thermal expansion and the glass transition. *Nat. Phys* 19:694–699. <https://doi.org/10.1038/s41567-022-01920-5>
153. Fahy GM, Wowk B (2015). Principles of cryopreservation by vitrification. In: Wolkers WF, Oldenhof H (eds) *Cryopreservation and freeze-drying protocols. Methods in Molecular Biology* 1257, Springer, New York, NY. https://doi.org/10.1007/978-1-4939-2193-5_2
154. Amini M, Benson JD (2023) Technologies for vitrification based cryopreservation. *Bioengineering* 10:508. <https://doi.org/10.3390/bioengineering10050508>
155. Abdelhady AW, Mittan-Moreau DW, Crane PL, McLeod MJ, Cheong SH, Thorne RE (2024) Ice formation and its elimination in cryopreservation of oocytes. *Sci Rep* 14:18809. <https://doi.org/10.1038/s41598-024-69528-8>
156. Takigawa T, Watanabe H, Akiyama Y (2024) Disaccharide-assisted inkjet freezing for improved cell viability. *Cryobiology* 116:104932. <https://doi.org/10.1016/j.cryobiol.2024.104932>
157. Joshi P, Taggart M, Uygun K, Sandlin RD (2024) Specimen containers and technologies for achieving vitrification through ultra-fast cooling. *Annu Rev Heat Transfer* 27:165–194. <https://doi.org/10.1615/AnnualRevHeatTransfer.2024056141>
158. Hopkins JB, Badeau R, Warkentin M, Thorne RE (2012) Effect of common cryoprotectants on critical warming rates and ice formation in aqueous solutions. *Cryobiology* 65:169–178. <https://doi.org/10.1016/j.cryobiol.2012.05.010>
159. Taylor MJ, Song YC, Brockbank KGM (2004) Vitrification in tissue preservation: new developments. In: Fuller BJ, Lane N, Benson EE (eds) *Life in the frozen*, State 629–668 CRC Press, 629–668. <https://doi.org/10.1201/9780203647073>
160. Huber AJ, Brockbank KG, Aberle T, Schleicher M, Chen ZZ, Greene ED, Lisy M, Stock UA (2012) Development of a simplified ice-free cryopreservation method for heart valves employing VS83, an 83% cryoprotectant formulation. *Biopreserv Biobank* 10:479–484. <https://doi.org/10.1089/bio.2012.0006>
161. Brockbank KGM, Chen Z, Greene ED, Campbell LH (2021) Vitrification of heart valve tissues. In: Wolkers WF, Oldenhof H (eds) *Methods in cryopreservation and freeze-drying*, *Methods in Molecular Biology*, Springer, 593–605. https://doi.org/10.1007/978-1-4939-2193-5_20
162. Jaskiewicz JJ, Callahan-Muller A, Gaby-Biegel N, Glover Z, Sandlin RD (2025) Validation of a high-throughput screening assay for the characterization of cryoprotective agent toxicity. *bioRxiv*, <https://doi.org/10.1101/2025.05.26.654916>
163. Ahmadkhani N, Sugden C, Benson JD, Eroglu A, Higgins AZ (2025) High-throughput evaluation of cryoprotective agents for mixture effects that reduce toxicity. *Cryobiology* 121:105316. <https://doi.org/10.1016/j.cryobiol.2025.105316>
164. Balcerzak AK, Capicciotti CJ, Briard JG, Ben RN (2014) Designing ice recrystallization inhibitors: from antifreeze (glyco)proteins to small molecules. *RSC Adv* 4:42682–42696. <https://doi.org/10.1039/C4RA06893A>
165. Chang T, Zhao G (2021) Ice inhibition for cryopreservation: materials, strategies, and challenges. *Adv Sci* 8:2002425. <https://doi.org/10.1002/advs.202002425>
166. Gangwar L, Han Z, Scheithauer C, Namsrai BE, Kantesaria S, Goldstein R, Etheridge ML, Finger EB, Bischof JC (2025) Physical vitrification and nanowarming at liter-scale CPA volumes: toward organ cryopreservation. *Nat Commun* 16:8511. <https://doi.org/10.1038/s41467-025-63483-2>
167. Powell-Palm MJ, Henley EM, Consiglio AN, Lager C, Chang B, Perry R, Fitzgerald K, Daly J, Rubinsky B, Hagedorn M (2023) Cryopreservation and revival of Hawaiian stony corals using isochoric vitrification. *Nat Commun* 14:4859. <https://doi.org/10.1038/s41467-023-40500-w>
168. Hagedorn M, Parenti LR, Craddock RA, Comizzoli P, Mabee P, Meinke B, Wolf SM, Bischof JC, Sandlin RD, Tessier SN, Toner M (2024) Safeguarding Earth's biodiversity by creating a lunar biorepository. *Bioscience* 74:561–566. <https://doi.org/10.1093/biosci/biae058>
169. Feys R, Uygun K, Filz von Reiterdank I, Wolf SM, Isasi R (2024) Biopreservation beyond the biosphere: exploring the ethical, legal & social implications of suspended animation in space. *J Law Med Ethics* 52:648–665. <https://doi.org/10.1017/jme.2024.148>
170. Best BP (2015) Cryoprotectant toxicity: facts, issues, and questions. *Rejuvenation Res* 18:422–436. <https://doi.org/10.1089/rej.2014.1656>
171. Jaskiewicz JJ, Callahan-Muller A, Gaby-Biegel N, Glover Z, Sandlin RD (2025) Validation of a high-throughput screening assay for the characterization of cryoprotective agent toxicity. *bioRxiv*, <https://doi.org/10.1101/2025.05.26.654916>
172. Hornberger K, Li R, Duarte ARC, Hubel A (2021) Natural deep eutectic systems for nature-inspired cryopreservation of cells. *AIChE J* 67:e17085. <https://doi.org/10.1002/aic.17085>
173. Mallya AS, Yadav P, Zakhia S, Hubel A (2025) Low-temperature characterization of sugar alcohol-based type V deep eutectic solvents for anti-icing and cryopreservation applications. *Sustain Chem Pharm* 48:102256. <https://doi.org/10.1016/j.scp.2025.102256>

174. Alvarez C, Berrospe-Rodriguez C, Wu C, Pasek-Allen J, Khosla K, Bischof J, Mangolini L, Aguilar G (2022) Photothermal heating of titanium nitride nanomaterials for fast and uniform laser warming of cryopreserved biomaterials. *Front Bioeng Biotechnol* 10:957481. <https://doi.org/10.3389/fbioe.2022.957481>
175. Oziri OJ, Rao JS, Scheithauer C, Han Z, Kantesaria S, Tobolt D, Liang H, Etheridge ML, Yin Y, Finger EB, Bischof JC (2025) Scalable purification of iron oxide nanoparticles for organ cryopreservation and transplantation. *Small* 21:e04910. <https://doi.org/10.1002/smll.202504910>